Local correlations in partially dual-unitary lattice models

Vladimir Al. Osipov [*]

Harbin Institute of Technology, 92 West Da Zhi Street, Harbin 150001, China

Niclas Krieger

Institute for Theoretical Physics, Plasma-Astroparticle Physics, Ruhr-University Bochum,
Universitätsstraße 150, 44801 Bochum, Germany
and Duisburg-Essen University, Lotharstraße 1, 47048 Duisburg, Germany

Thomas Guhr

Duisburg-Essen University, Lotharstraße 1, 47048 Duisburg, Germany

Boris Gutkin

H.I.T.-Holon Institute of Technology, 52 Golomb Street, POB 305, Holon 5810201, Israel

We consider the problem of local correlations in the kicked, dual-unitary coupled maps on D-dimensional lattices. We demonstrate that for $D \geqslant 2$, fully dual-unitary systems exhibit ultralocal correlations: The correlations between any pair of operators with a local support vanish in a finite number of time steps. In addition, for $D = 2$, we consider the partially dual-unitary regime of the model, where the dual-unitarity applies to only one of the two spatial directions. For this case, we show that correlations generically decay exponentially and provide an explicit formula for the correlation function between the operators supported on two and four neighboring sites.

I. INTRODUCTION

Until recently, the vast majority of research in the field of quantum chaos has been limited to systems with few degrees of freedom, even though chaotic spectral statistics were first found in the atomic nuclear, which essentially is a many-body problem [1,2]. Indeed, the many-body quantum systems, where the Hilbert space dimension grows exponentially with the number of degrees of freedom, represent a significant challenge for numerical and analytical studies. In recent years substantial progress in the field has been achieved due to the introduction of new classes of many-body models and the development of appropriate mathematical methods for their investigation. This is closely connected to a burst of activities in the field of quantum circuits, see a recent review in [3]. In this article, our attention is focused on the calculation of the correlations between localized quantum observables in dual-unitary quantum systems of arbitrary dimensions, with a particular focus on $D = 2$ dimensions. Dual-unitary models possess a remarkable property—their dynamics are invariant under the exchange of spatial and temporal degrees of freedom. A toy model with such property, a chain of linearly coupled Arnold's cat maps, was first introduced in [4] and subsequently studied in a number of papers [5–7] both on classical and quantum levels. Other examples of dual-unitary

models were found among different classes of systems, e.g., kicked Ising spin chain and its generalizations [8–11], circuit lattices [12–15]. Although their full characterisation is still absent, dual-unitary models are generic and can be constructed in a systematic way [16].

In the field of many-body quantum chaos the dual-unitary models attract considerable attention [8–10,12,16–26] due to their intriguing properties. On one hand, they demonstrate quantum properties akin to those of maximally chaotic many-body systems, such as Wigner-Dyson spectral statistics and insusceptibility to many-body localization effects [9,19,27]. On the other hand, dual-unitary models are amenable to exact treatment. In particular, due to the combination of duality and causality, the local two-point correlation functions in these systems can be calculated exactly [11,12,28]. Correlations continue to find considerable interest [22,29–34]. Other recent research directions include aspects of matrix product states [20,35], steady states as well as eigenstate thermalization [36,37], computational aspects [38], and random matrix statistics [39,40].

Previous studies have primarily focused on dual-unitary models with a single spatial dimension. Extension to two spatial dimensions has been considered in a number of recent papers [13,14,38,41] for quantum circuits model. In the current study, we extend our investigation to encompass coupled map lattices of an arbitrary dimension D. Our findings reveal that starting from $D = 2$ onwards, the correlations within a system exhibiting the complete spatiotemporal symmetry

---
[*]Vladimir.Al.Osipov@gmail.com

demonstrate an ultralocal behavior, which implies that the correlations between operators with local support vanish identically after a finite time. In particular, this suggests that in the case $D \geqslant 2$, the requirement of the complete duality can be relaxed without compromising the solvability of the model. Accordingly, in the main body of this paper, we consider partially dual -unitary map lattices, where the system remains invariant under the exchange of the time variable and only one of several spatial coordinates. Dual-unitary quantum circuits of this type have recently been explored in [38], where it has been demonstrated that correlation functions are classically simulatable for certain types of initial states. The central result of the present paper is the explicit expression for the local correlation function in the partially dual-unitary coupled maps. The way of derivation is closely related to the one suggested in Ref. [11].

II. THE MAIN IDEAS

The general model considered in this paper is defined for a finite piece of the D-dimensional lattice $\mathbb{Z}^D$. Specifically, let $\bar{\mathbb{Z}}^D$ be a finite-size hyper rectangular subset of $\mathbb{Z}^D$ where N_i (for $i = 1, \ldots, D$) represents the number of sites along the ith spatial direction so that the product $\mathcal{N} = N_1 \cdot N_2 \cdots \cdot N_D$ is the total number of sites of the lattice $\bar{\mathbb{Z}}^D$. The unitary Floquet evolution operator U acts in discrete time steps in the Hilbert space $\mathcal{H}^{\otimes \mathcal{N}}$, which is the tensor product of $\mathcal{N}$ local L-dimensional spaces $\mathcal{H} = \mathbb{C}^L$. In the following, we assume that the time evolution U is dual unitary (at least for one spatial direction) with a unit speed of interaction propagation. Detailed information regarding the construction of U with the necessary properties will be provided in the main body of the paper.

The main object of our consideration is the reduced correlation function between two local observables, $\hat{Q}_1$ and $\hat{Q}_2$ after t time steps of the evolution,

$$C(\boldsymbol{r}, t) = \langle \hat{Q}_1(0)\hat{Q}_2(t) \rangle - \langle \hat{Q}_1(0) \rangle \langle \hat{Q}_2(t) \rangle, \quad (2.1)$$

where the evolution is provided by the action of a unitary operator U,

$$\hat{Q}_i(t) = U^{-t} Q_i U^t, \quad i = 1, 2. \quad (2.2)$$

It is important to note that the value of t should be smaller than any spatial dimension of $\bar{\mathbb{Z}}^D$, ensuring that the resulting correlation function remains independent of both the size of $\bar{\mathbb{Z}}^D$ and the boundary conditions. To make our explanations more transparent we assume here that two observables, Q_1 and Q_2, are strictly local. In other words, they are localized at single lattice points $\boldsymbol{r}_1 \in \bar{\mathbb{Z}}^D$, and $\boldsymbol{r}_2 \in \bar{\mathbb{Z}}^D$, respectively. Furthermore, since our model is shift invariant, the correlation function depends solely on the difference $\boldsymbol{r} = \boldsymbol{r}_2 - \boldsymbol{r}_1$. Consequently, we can set, without a loss of generality, that Q_1 is localized at the origin $\mathbf{0}$ and Q_2 at the position $\boldsymbol{r}$, respectively. The average in Eq. (2.1) is defined by the operator trace taken over the entire many-body Hilbert space, $\langle \cdot \rangle = L^{-D} \text{Tr} (\cdot)$.

To explain the main ideas of the paper we will now consider the cases of one-dimensional ($D = 1$) and two-dimensional lattices ($D = 2$).
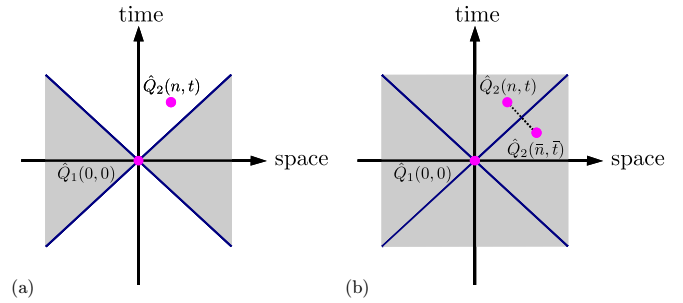

FIG. 1. Representation of the connected part of the correlation function $C(n, t)$ [Eq. (2.1)] between two observables located at the coordinates $(0,0)$ and (n, t) of the space-time grid. (a) In the general case due to causality the correlations vanish inside the light cones defined by the inequality $|n| > |t|$ (grey regions). (b) In the case of the dual-unitary model, when Eq. (2.3) holds, solely the correlations along the light-cone edges (dark-blue lines $|n| = |t|$) do not vanish.

A. One-dimensional lattice (chain) of quantum maps

For a one-dimensional lattice (chain) $\bar{\mathbb{Z}}^1$, the location of an observable is determined by an integer number n, $\boldsymbol{r} = n$. Since the speed of interaction propagation equals one, the causality implies that the correlation function of many-body operators (2.1) vanishes outside the light cone $|t| < |n|$, see Fig. 1(a). Furthermore, for dual unitary U, the correlation function remains invariant under exchange of time t and the spatial coordinate n,

$$C(n, t) = C(t, n). \quad (2.3)$$

Therefore, the correlation function $C(n, t)$ nullifies also inside the light cone $|n| < |t|$, see Fig. 1(b). As a result, the light-cone edges $|t| = |n|$ remain as the only possible location of the space-time manifold where the nontrivial correlations can arise. From a technical point of view, the calculation of the correlation function in the dual-unitary case reduces to the calculation of the correlations propagating along the light-cone edges, which in turn can be expressed through an expectation value of a product of transfer matrices of a reduced dimension, independent on D, see [11,12,28].

B. Two-dimensional lattice of quantum maps

In the case of a two-dimension lattice $\bar{\mathbb{Z}}^2$ the situation is somewhat different. Here any point of the lattice is labeled by a pair of integers $\boldsymbol{r} = (m, n)$. Due to causality, the correlations vanish outside the light-cone domain

$$|t| \geqslant |n| + |m|, \quad (2.4)$$

see Fig. 2. For systems with full spatiotemporal symmetry, the correlation function remains invariant under the exchange of t and n, as well as under the exchange of t and m. This implies that for the nontrivial correlations the inequalities

$$|m| \geqslant |n| + |t|, \quad |n| \geqslant |t| + |m| \quad (2.5)$$

must hold, as well. It is straightforward to see that the only point satisfying all three inequalities [(2.4) and (2.5)] is the origin of the space-time grid $t = m = n = 0$. In other words, all correlations of strictly local operators vanish for any time $t > 0$. A similar consideration for the operators supported
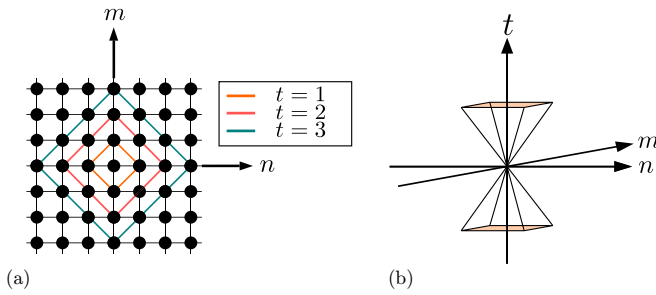
FIG. 2. On the left (a) is shown a lattice $\bar{\mathbb{Z}}^D$ with a central point located at the origin ($n = 0, m = 0$) of the system. The lines $t = 1$ (orange), $t = 2$ (red), and $t = 3$ (blue) mark the event horizon of the light cone. The observables, which are outside the cone at a given time step t, do not correlate with the observable at the origin. The right figure (b) shows the entire light cone with the boundaries of the event horizon represented by the eight triangular areas.

on a finite number ℓ of sites shows that $C(\boldsymbol{r}, t) = 0$ for $t > \ell$. For this reason, we refer to such behavior as ultralocal correlations.

Note that the "light-cone" borders are determined by the velocity of the signal propagation. Generically the light-cone surface can be seen as a space-time membrane pinned to the initial point, so that its surface tension is interpreted in terms of the rate at which information "flows" across it. This allows to consider generic (nonunitary) dynamics across the membrane [15]. Note also that the ultralocal behavior of the correlation function in our model contrasts with that of the correlation function in the ternary-unitary and triunitary $(2 + 1)$-dimensional circuits introduced in [13] and [41], respectively. In these models, the light-cone domain is determined by the conditions: $|t| \geqslant |n|$, $|t| \geqslant |m|$. Application of the above duality argument in this case yields nontrivial correlations along the lines $|t| = |n| = |m|$. In Appendix A, we show that a dual-unitary kicked quantum map on 2D lattice can be represented as a 2D quantum circuit with a ternary unitary gate operator as described in [41] and give explanation to the seeming ambiguity mentioned above.

Suppose now that our system belongs to a class of partially dual-unitary systems. It is invariant under the exchange of only one coordinate, e.g., n and time t. In such a case the domain of nontrivial correlations is given by

$$|t| \geqslant |n| + |m| \cap |n| \geqslant |t| + |m|. \qquad (2.6)$$

The correlation function $C(\boldsymbol{r}, t)$ does not necessarily vanish along the line $m = 0$, $|n| = |t|$. In the body of the text, we show, similarly to the one-dimensional case, that the correlations along this line can be expressed through an expectation value of a transfer operator powers. In particular, the transfer operator eigenvalues determine the decay rates of the correlations.

C. Outline of the article

In the next section, we formulate the general model of coupled quantum maps with periodic kicks in D spatial dimensions. In this context, we introduce the notion of partial and full dual unitarity. In Sec. IV we briefly recall the main results for $D = 1$ case. We then introduce the correlation

function for the $D = 2$ model and demonstrate that, similar to the one-dimensional case, it can be expressed in the form of a three-dimensional partition function for a classical spin model. In Sec. V, we derive the contraction rules that enable us to compute the correlation function. The general expressions for the transfer operator and the correlation function are derived in Sec. VI. In Sec. VII we apply our results to the model of coupled cat maps and kicked Ising spin lattice. For this purpose we study here in detail the spectra of the corresponding transfer operators. Finally, in Sec. VIII we give the concluding remarks.

III. THE KICKED QUANTUM MAP ON A LATTICE

To start our consideration we introduce a multidimensional lattice model of periodically kicked locally interacting particles. The system Hamiltonian $H(t)$ consists of the time-dependent and the time-independent parts,

$$H(t) = H_I + H_K \sum_{\tau=-\infty}^{+\infty} \delta(t - \tau). \qquad (3.1)$$

The kick part of the Hamiltonian H_K induces independent evolution of noninteracting particles. It turns on periodically at integer instants of time τ. The H_I part [Eq. (3.1)] describes the nearest-neighbor interaction between the particles. Such Hamiltonian structure, in particular, implies that the quantum time evolution can be written as a product

$$U = U_K U_I \qquad (3.2)$$

of unitary evolutions [8,42,43] U_K and U_I, corresponding to the kick and the interaction parts of the Hamiltonian, respectively.

To specify the form of the unitary operators we define, first, the on-site local Hilbert space $\mathcal{H}$ equipped with the discrete L-dimensional basis $\{|s\rangle, \ s = \overline{1, L}\}$. The total Hilbert space of the system is defined then by the tensor product $\mathcal{H}^{\otimes \mathcal{N}}$. It has the dimension $L^{\mathcal{N}}$ and possesses the natural product basis,

$$\left\{ |\boldsymbol{s}\rangle \equiv \prod_{j \in \bar{\mathbb{Z}}^D} |s_j\rangle, \ s_j = \overline{1, L} \right\}, \qquad (3.3)$$

where the multidimensional index $\boldsymbol{j}$ marks the particles' positions in the lattice $\bar{\mathbb{Z}}^D$ and the product runs over all $\mathcal{N}$ lattice sites. The Floquet time evolution between the kicks is governed by the unitary operator $U_I = e^{-iH_I}$. We require that H_I couples the nearest neighbor sites of the multidimensional lattice and has to be diagonal in the product basis (3.3). This yields the following matrix form of the evolution operator:

$$\langle \boldsymbol{s}|U_I[\boldsymbol{f}]|\boldsymbol{s}'\rangle = \delta(\boldsymbol{s}, \boldsymbol{s}') \exp\left[i \sum_{d=1}^{D} \sum_{\boldsymbol{j}} f_d(s_{\boldsymbol{j}}, s_{\boldsymbol{j}+\mathbf{1}_d}) \right], \qquad (3.4)$$

where $U_I[\boldsymbol{f}]$ is determined by the set of functions $\boldsymbol{f} = (f_1, f_2, \ldots, f_D)$. Here we used the notation $\mathbf{1}_d$, which denotes the one site shift of the index $\boldsymbol{j}$ in the spatial direction d. The function $\delta(\boldsymbol{s}, \boldsymbol{s}')$ stands for the product of the Kronecker

symbols, $\delta(\boldsymbol{s}, \boldsymbol{s}') = \prod_j \delta(s_j, s_j')$. In the above formula [Eq. (3.4)] the cyclic boundary conditions in each spatial dimension are implied. The operator U_I acts independently in each spatial direction so that it can be represented as a product of mutually commuting unitary operators U_{I_d}, where d indexes the spatial axis number,

$$U_I[\boldsymbol{f}] = \prod_{d=1}^{D} U_{I_d}, \qquad (3.5)$$

$$\langle \boldsymbol{s} | \prod_{d=1}^{D} U_{I_d} | \boldsymbol{s}' \rangle = \delta(\boldsymbol{s}, \boldsymbol{s}') L^{\mathcal{N}/2} \prod_{d=1}^{D} \prod_j \langle s_j | u[f_d] | s_{j+1_d} \rangle, \quad (3.6)$$

where we have introduced the notation $u[f]$ for the $L \times L$ unitary matrix with the symbol f, and the factor $L^{\mathcal{N}/2}$ is introduced to satisfy the unitary properties of $u[f]$. Its entries are

$$\langle s | u[f] | s' \rangle = \frac{1}{\sqrt{L}} e^{\mathrm{i}f(s,s')}, \qquad (3.7)$$

and the unitarity condition is written in the form

$$\frac{1}{L} \sum_{s'=1}^{L} e^{\mathrm{i}f(s,s')} e^{-\mathrm{i}f^*(s'',s')} = \delta(s, s''). \qquad (3.8)$$

Note that, to satisfy the unitary condition for U_I, each function f_d in Eqs. (3.4) and (3.6) has to be a real-valued function.

The kick part H_K of the total Hamiltonian H in Eq. (3.1) defines the on-site particle dynamics. The corresponding evolution operator $U_K = e^{-\mathrm{i}H_K}$ can be represented as the tensor product of unitary operators defined in the single-particle Hilbert space. We assume that the kicks act identically on each particle, so that

$$\langle \boldsymbol{s} | U_K[g] | \boldsymbol{s}' \rangle = \prod_j \langle s_j | u[g] | s_j' \rangle, \qquad (3.9)$$

where u is the $L \times L$ unitary matrix with the symbol g. Matrix $u[g]$ satisfies the unitarity condition

$$\frac{1}{L} \sum_{s'=1}^{L} e^{\mathrm{i}g(s,s')} e^{-\mathrm{i}g^*(s'',s')} = \delta(s, s''). \qquad (3.10)$$

Having introduced the basic notations we are in a position to formulate the duality relation for the quantum maps, which has been established for the one-dimensional case in Ref. [11]. In the case $D = 1$ it states that for the dual-unitary quantum system the evolution operator $U = U_K[g]U_I[f]$ and its dual counterpart, $\tilde{U} = U_K[f]U_I[g]$, obtained by the exchange of f and g functions, are both unitary and the system possesses the spatiotemporal symmetry. Note that this requires the Hadamard property for the matrices

$$\langle s | u[f] | s' \rangle = \frac{e^{\mathrm{i}f(s,s')}}{\sqrt{L}}, \quad \langle s | u[g] | s' \rangle = \frac{e^{\mathrm{i}g(s,s')}}{\sqrt{L}}. \qquad (3.11)$$

In other words, these are $L \times L$ unitary matrices with identical absolute values for all entries, where both f and g are real-valued functions. Certainly the duality is achieved when $f = g$, so that $U \equiv \tilde{U}$. As we demonstrate in Sec. VII. (applications) the strict equivalence $f = g$ is not necessary for the

duality. In fact, f and g can be chosen from rather wide class of functions.

The above notion of dual unitarity can be straightforwardly extended to an arbitrary dimension D. In general, there exist D possible dual operators,

$$\tilde{U}_j = U_K[f_j]U_I[\tilde{\boldsymbol{g}}], \quad \tilde{\boldsymbol{g}} = (f_1, \ldots, g, \ldots, f_D), \qquad (3.12)$$

where the function g is exchanged with one of the spatial coupling functions f_j. We say that the system is partially dual unitary if one of the spatial evolution operators $\tilde{U}_j$ is unitary. The system is called fully dual unitary if all $\tilde{U}_j$, $j = 1, \ldots, D$ are unitary. If, in addition all functions f_j, $j = 1, \ldots, D$ and g are equal, then

$$U = \tilde{U}_1 = \tilde{U}_2 = \cdots = \tilde{U}_D.$$

In this case, the system possesses full spatiotemporal symmetry.

IV. CORRELATIONS BETWEEN LOCAL OPERATORS

In this paper, we aim at the calculation of the correlation function,

$$C(t) = L^{-\mathcal{N}} \operatorname{Tr} \bar{\Sigma} U^{-t} \underline{\Sigma} U^t, \qquad (4.1)$$

for two local observables $\bar{\Sigma}$, $\underline{\Sigma}$. For simplicity of exposition, we restrict our consideration to the case of two-dimensional spatial lattices $\bar{\mathbb{Z}}^2$, while the generalization to D-dimensional lattices with $D > 2$ is straightforward.

A. One-dimensional lattice

We start by recalling the results of [11] for the one-dimensional case. There the correlation function (4.1) was calculated for the operators $\bar{\Sigma}$ and $\underline{\Sigma}$ given by the products of the following form:

$$\bar{\Sigma} = \mathbf{q}_1 \otimes \mathbf{q}_2 \otimes \underbrace{\mathbb{1} \otimes \cdots \otimes \mathbb{1}}_{N-2}, \qquad (4.2)$$

$$\underline{\Sigma} = \underbrace{\mathbb{1} \otimes \cdots \otimes \mathbb{1}}_{n} \otimes \mathbf{q}_3 \otimes \mathbf{q}_4 \otimes \underbrace{\mathbb{1} \otimes \cdots \otimes \mathbb{1}}_{N-n-2}, \qquad (4.3)$$

where each $\mathbf{q}_\ell$ ($\ell = 1, 2, 3, 4$) is an operator acting on the on-site Hilbert space $\mathcal{H}$.

For the one-dimensional ($D = 1$) dual-unitary model the correlation function (4.1) for the traceless $\mathbf{q}_\ell$ always equals zero, except for the case when the correlations are considered along the "light-cone" edge. The latter case corresponds to the choice $|n| = t$ in Eq. (4.3). The resulting correlation function at the light-cone edge, $n = t > 2$, can be represented as the expectation value of the transfer operator $\hat{\boldsymbol{T}}$ power,

$$C_{D=1}(t) = \langle \bar{\boldsymbol{\Phi}}_{\mathbf{q}_1, \mathbf{q}_2} | \hat{\boldsymbol{T}}^{t-2} | \boldsymbol{\Phi}_{\mathbf{q}_3, \mathbf{q}_4} \rangle, \qquad (4.4)$$

where the vectors $\langle \bar{\boldsymbol{\Phi}}_{\mathbf{q}_1, \mathbf{q}_2} |$, $| \boldsymbol{\Phi}_{\mathbf{q}_3, \mathbf{q}_4} \rangle$ depend on the operators $\mathbf{q}_1$, $\mathbf{q}_2$, and $\mathbf{q}_3$, $\mathbf{q}_4$, respectively. The transfer operator $\hat{\boldsymbol{T}}$ acts in the Hilbert space $\mathcal{H} \otimes \mathcal{H}$, and has the entries

$$\langle \chi, \eta | \hat{\boldsymbol{T}} | \chi', \eta' \rangle = \frac{1}{L^3} \left| \sum_{s=1}^{L} e^{\mathrm{i}f_1(\chi,s) + \mathrm{i}g(\eta,s) + \mathrm{i}g(s,\chi') + \mathrm{i}f_1(s,\eta')} \right|^2. \qquad (4.5)$$

In a general nondual case the correlation function becomes zero only outside the light cone, $|n| > t$ (which is supported by the argument that the speed of information propagation in the kicked chain model equals 1), but remains finite inside the light cone, $|n| < t$.

The result (4.4) was obtained in [11] by representing the correlation function $C(t)$ in the form of a partition function of a classical spin lattice model, followed by the application of contraction rules that allow the elimination of most of the spin variables. As we demonstrate below, this method also applies to the higher dimensional lattices.

B. Two-dimensional lattice

We now consider the correlation function (4.1) for two-dimensional lattice models. For convenience we address two spatial directions as "vertical" and "horizontal", using indexes v and h, instead of 1 and 2. The number of sites in the vertical and horizontal direction is denoted by N and M, respectively, with $\mathcal{N} = MN$ being the total number of lattice sites. The two-point correlation function is defined by Eq. (4.1) with the evolution matrix $U = U_K U_I$, where the interaction part of the

evolution operator,

$$\langle s|U_I|s'\rangle \equiv \delta(s, s') \prod_{n=1}^{N} \prod_{m=1}^{M} e^{i f_v(s_{n,m}, s_{n+1,m}) + f_h(s_{n,m}, s_{n,m+1})}, \quad (4.6)$$

is diagonal in the product basis $|s\rangle$. The circular boundary conditions are assumed in the above formulas, namely, $s_{n,M+1} \equiv s_{n,1}$, and $s_{N+1,m} \equiv s_{1,m}$. The kicked part of the evolution is defined by the Eqs. (3.7) and (3.9).

We consider correlations (4.1) for a pair of many-body operators $\bar{\Sigma}$ and $\underline{\Sigma}$, each supported at four neighboring points of the lattice. They are defined by eight [rather than four, as in Eqs. (4.2) and (4.3)] local matrices $\mathbf{q}_\ell$, $\ell = 1, \ldots, 8$. Without loss of generality, we define $\bar{\Sigma}$ as a direct product, where the nontrivial matrices are placed in the "left upper corner", i.e., at the coordinates $(n, m) = \{(1, 1), (1, 2), (2, 1), (2, 2)\}$. The second many-body operator, $\underline{\Sigma}$ has the nontrivial entries at the coordinates $(n, m) = \{(v, \mu), (v, \mu + 1), (v + 1, \mu), (v + 1, \mu + 1)\}$. Schematically, these operators can be represented as follows:

$$
\bar{\Sigma} =
\begin{array}{cccccccccc}
 & 1 & & 2 & & 3 & & & N & \\
\hline
\mathbf{q}_1 & \otimes & \mathbf{q}_2 & \otimes & \mathbb{1} & \otimes & \ldots & \otimes & \mathbb{1} & \otimes & 1 \\
\mathbf{q}_3 & \otimes & \mathbf{q}_4 & \otimes & \mathbb{1} & \otimes & \ldots & \otimes & \mathbb{1} & \otimes & 2 \\
\mathbb{1} & \otimes & \mathbb{1} & \otimes & \mathbb{1} & \otimes & \ldots & \otimes & \mathbb{1} & \otimes & 3 \\
 & & & & & \vdots & & & & \\
\mathbb{1} & \otimes & \mathbb{1} & \otimes & \mathbb{1} & \otimes & \ldots & \otimes & \mathbb{1} & & M
\end{array},
$$

$$
\underline{\Sigma} =
\begin{array}{ccccccccccc}
 & v-1 & & v & & v+1 & & v+2 & & \\
\hline
\vdots & & \vdots & & \vdots & & \vdots & & & \\
\ldots \otimes & \mathbb{1} & \otimes & \mathbb{1} & \otimes & \mathbb{1} & \otimes & \mathbb{1} & \otimes \ldots & \mu - 1 \\
\ldots \otimes & \mathbb{1} & \otimes & \mathbf{q}_5 & \otimes & \mathbf{q}_6 & \otimes & \mathbb{1} & \otimes \ldots & \mu \\
\ldots \otimes & \mathbb{1} & \otimes & \mathbf{q}_7 & \otimes & \mathbf{q}_8 & \otimes & \mathbb{1} & \otimes \ldots & \mu + 1 \\
\ldots \otimes & \mathbb{1} & \otimes & \mathbb{1} & \otimes & \mathbb{1} & \otimes & \mathbb{1} & \otimes \ldots & \mu + 2 \\
\vdots & & \vdots & & \vdots & & \vdots & & &
\end{array}. \quad (4.7)
$$

To evaluate the correlation function, we first introduce the basis vectors additionally indexed by the integer time t,

$$|s_t\rangle \equiv \prod_{(n,m) \in \bar{\mathbb{Z}}^2} |s_{nmt}\rangle, \quad (4.8)$$

and then write

$$C(T) \equiv L^{-\mathcal{N}} \mathrm{Tr}\, \bar{\Sigma} U^{-T} \underline{\Sigma} U^T = L^{-\mathcal{N}} \sum \langle s_{2T+1}|\bar{\Sigma}|s_0\rangle \langle s_T|\underline{\Sigma}|s_{T+1}\rangle \left(\prod_{t=0}^{T-1} \langle s_t|U^\dagger|s_{t+1}\rangle \langle s_{2T-t}|U|s_{2T-t+1}\rangle \right), \quad (4.9)$$

where the sum runs over all possible values of the components, $s_{nmt} \in \overline{1, L}$. We assume that for $T = 0$ the product in Eq. (4.9) equals 1 identically. It is also convenient to introduce at each position (m, n) a two-component spin variable with the components $\bar{s}_{nmt}$ and $\underline{s}_{nmt}$. The upper component of the spin variable $\bar{s}_{n,m,t}$ coincides with $s_{n,m,t}$ for all $t \in \overline{0, T}$. The lower component corresponds to the spin variable taken at the conjugated instance of time $2T - t$, such that $\underline{s}_{n,m,t} = s_{n,m,2T-t+1}$ with the same set of the indexes $t \in \overline{0, T}$. The schematics of the above correspondence are plotted below for convenience

$$
\begin{array}{ccccccccccccc}
s_0 & & & s_{T-1} & & s_T & | & s_{T+1} & & s_{T+2} & & & s_{2T+1} \\
\bullet & \Leftrightarrow & \ldots & \bullet & \Leftrightarrow & \bullet & | & \bullet & \Leftrightarrow & \bullet & \ldots & \Leftrightarrow & \bullet \\
\bar{s}_0 & & & \bar{s}_{T-1} & & \bar{s}_T & | & \underline{s}_T & & \underline{s}_{T-1} & & & \underline{s}_0
\end{array}. \quad (4.10)
$$

Using this notation we can rewrite the correlation function in a symmetric form,

$$C(T) = L^{-\mathcal{N}} \sum_{\mathbf{S}} \bar{\Phi}(\bar{s}_0, \underline{s}_0) \bar{T}_I(\bar{s}_0, \underline{s}_0) \Phi(\bar{s}_T, \underline{s}_T)$$

$$\times \prod_{t=0}^{T-1} \bar{T}_K(\bar{s}_t, \bar{s}_{t+1}; \underline{s}_{t+1}, \underline{s}_t) \bar{T}_I(\bar{s}_{t+1}, \underline{s}_{t+1}), \quad (4.11)$$

where $\bar{\Phi}$ and Φ depend on $\mathcal{N}$ spin variables and implicitly include dependence on the matrices q_ℓ,

$$\bar{\Phi}(\underline{s}_0, \bar{s}_0) = \langle \underline{s}_0 | \bar{\Sigma} | \bar{s}_0 \rangle, \quad (4.12)$$

$$\Phi(\bar{s}_T, \underline{s}_T) = \langle \bar{s}_T | U_I \underline{\Sigma} U_I^\dagger | \underline{s}_T \rangle. \quad (4.13)$$

Each $\bar{T}_I$ is a function of $\mathcal{N}$ spin variables and describes the particle interactions between the kicks. Substituting the explicit form of the matrix U_I entries [Eq. (4.6)] we have for $\bar{T}_I$,

$$\bar{T}_I(\bar{s}_t, \underline{s}_t) \equiv \langle \bar{s}_t | U_I | \bar{s}_t \rangle^* \langle \underline{s}_t | U_I | \underline{s}_t \rangle$$

$$= \prod_{n=1}^N \prod_{m=1}^M e^{-i f_v(\bar{s}_{n,m,t}, \bar{s}_{n+1,m,t}) + i f_v(\underline{s}_{n,m,t}, \underline{s}_{n+1,m,t})}$$

$$\times e^{-i f_h(\bar{s}_{n,m,t}, \bar{s}_{n,m+1,t}) + i f_h(\underline{s}_{n,m,t}, \underline{s}_{n,m+1,t})}. \quad (4.14)$$

The explicit form of the matrix U_K [Eqs. (3.9) and (3.7)] allows to write down the expression for $\bar{T}_K$,

$$\bar{T}_K(\bar{s}_t, \bar{s}_{t+1}; \underline{s}_{t+1}, \underline{s}_t)$$

$$\equiv \langle \bar{s}_{t+1} | U_K | \bar{s}_t \rangle^* \langle \underline{s}_{t+1} | U_K | \underline{s}_t \rangle$$

$$= \frac{1}{L^{NM}} \prod_{n=1}^N \prod_{m=1}^M e^{-i g^*(\bar{s}_{n,m,t+1}, \bar{s}_{n,m,t}) + i g(\underline{s}_{n,m,t+1}, \underline{s}_{n,m,t})}. \quad (4.15)$$

The sum runs over all possible values of the full set

$$\mathbf{S} = \{(\bar{s}_{nmt}, \underline{s}_{nmt}) | (n, m, t) \in \mathcal{L}\}, \quad (4.16)$$

of the $MNT \equiv |\mathbf{S}|$ spin variables, located at the nodes of the 3D space-time grid,

$$\mathcal{L} = \{(n, m, t) | t \in \overline{0, T}, n \in \overline{1, N}, m \in \overline{1, M}\}. \quad (4.17)$$

Note that in the present calculations, we have used the symmetrization procedure slightly different than in Ref. [11]. Namely, instead of incorporating U_I into $\bar{\Phi}$ we introduced an additional unity operator $\mathbb{1} = U_I U_I^\dagger = U_I^\dagger U_I$ from both sides of $\underline{\Sigma}$. This is done to formulate the contraction rules in a symmetric way.

The correlation function (4.11) can be equally represented in another form with the structure of a partition function,

$$C(T) = \frac{1}{L^{|\mathbf{S}|}} \sum_{\mathbf{S}} G_1(\mathbf{S}_1) G_2(\mathbf{S}_2) e^{-i\mathcal{F}(\mathbf{S})}. \quad (4.18)$$

The expression under the sum is split into the product of three factors in accordance with the location of the spin variables within the lattice $\mathcal{L}$. The first one is given by $G_1(\mathbf{S}_1) = D_{\bar{\Sigma}} D_{\underline{\Sigma}}$, where

$$D_{\bar{\Sigma}} = \langle \bar{s}_{111} | u[g] \mathbf{q}_1 u^\dagger[g] | \underline{s}_{111} \rangle \langle \bar{s}_{121} | u[g] \mathbf{q}_2 u^\dagger[g] | \underline{s}_{121} \rangle$$

$$\times \langle \bar{s}_{211} | u[g] \mathbf{q}_3 u^\dagger[g] | \underline{s}_{211} \rangle \langle \bar{s}_{221} | u[g] \mathbf{q}_4 u^\dagger[g] | \underline{s}_{221} \rangle, \quad (4.19)$$

$$D_{\underline{\Sigma}} = \langle \bar{s}_{\nu\mu T} | \mathbf{q}_5 | \underline{s}_{\nu\mu T} \rangle \langle \bar{s}_{\nu\mu+1 T} | \mathbf{q}_6 | \underline{s}_{\nu\mu+1 T} \rangle$$

$$\times \langle \bar{s}_{\nu+1\mu T} | \mathbf{q}_7 | \underline{s}_{\nu+1\mu T} \rangle \langle \bar{s}_{\nu+1\mu+1 T} | \mathbf{q}_8 | \underline{s}_{\nu+1\mu+1 T} \rangle. \quad (4.20)$$

It depends on the spin variables

$$\mathbf{S}_1 = \{(\bar{s}_{nmt}, \underline{s}_{nmt}) | (n, m, t) \in \mathcal{L}_1\}, \quad (4.21)$$

located at the eight lattice sites,

$$\mathcal{L}_1 = \{(1, 1, 1), (1, 2, 1), (2, 1, 1), (2, 2, 1), (\nu, \mu, T),$$
$$(\nu, \mu + 1, T), (\nu + 1, \mu, T), (\nu + 1, \mu + 1, T)\}, \quad (4.22)$$

corresponding to the position of the local operators $\mathbf{q}_\ell$ in $\bar{\Sigma}$, $\underline{\Sigma}$. The second term is given by the product of the Kronecker delta functions

$$G_2(\mathbf{S}_2) = \prod_{(n,m,t) \in \mathcal{L}_2} \delta(\bar{s}_{nmt}, \underline{s}_{nmt}). \quad (4.23)$$

It depends on the spin variables

$$\mathbf{S}_2 = \{(\bar{s}_{nmt}, \underline{s}_{nmt}) | (n, m, t) \in \mathcal{L}_2\}, \quad (4.24)$$

located at the subset

$$\mathcal{L}_2 = \{(n, m, t) | t \in \{1, T\}, n \in \overline{1, N}, m \in \overline{1, M}\} \setminus \mathcal{L}_1$$

of the three-dimensional space-time grid. Finally, the interaction between spins is described by the third term $e^{-i\mathcal{F}(\mathbf{S})}$, where the exponent is given by the function

$$\mathcal{F} = \sum_{(n,m,t) \in \mathcal{L}} f_v(\bar{s}_{n,m,t}, \bar{s}_{n+1,m,t}) + f_v(\underline{s}_{n,m,t}, \underline{s}_{n+1,m,t})$$

$$+ f_h(\bar{s}_{n,m,t}, \bar{s}_{n,m+1,t}) + f_h(\underline{s}_{n,m,t}, \underline{s}_{n,m+1,t})$$

$$+ g^*(\bar{s}_{n,m,t+1}, \bar{s}_{n,m,t}) + g(\underline{s}_{n,m,t+1}, \underline{s}_{n,m,t}), \quad (4.25)$$

and the sum runs over the full set $\mathbf{S}$ of spin variables.

V. GRAPHICAL METHOD FOR EVALUATION OF CORRELATIONS

The correlation function, expressed in the form of the partition function (4.18) permits an instructive graphical representation, as illustrated in Fig. 3. The 3D space-time lattice $\mathcal{L}$ is partitioned into the three subsets $\mathcal{L}_1, \mathcal{L}_2, \mathcal{L}_3 \equiv \mathcal{L}/(\mathcal{L}_1 \cup \mathcal{L}_2)$. In the picture, the spin variables are schematically shown by balls of various colors in accordance with their role in the partition function (4.18). The green-colored balls, located at $\mathcal{L}_1$, correspond to the positions of the operators $\mathbf{q}_\ell$, see Eq. (4.7). The red balls, located at the subset $\mathcal{L}_2$, correspond to the δ-correlated spins. Since each unit matrix $\mathbb{1}$ in the operators $\bar{\Sigma}$ and $\underline{\Sigma}$ generates the pair of the δ-correlated spins, the majority of the endpoints are colored red. Finally, the brown balls placed at $\mathcal{L}_3$ correspond to all other spin variables.

In general, the partition function (4.18) can be calculated by eliminating the spin variables one by one. To facilitate this procedure, a simple graphical method can be developed by drawing an analogy with Ref. [11]. Below, we formulate the "contraction rules", which form the basis of our approach.

A. Contraction rules

Consider the local configuration consisting of four neighboring δ-correlated spins and an unpaired spin $(\bar{s}_{n,m,t+1}, \underline{s}_{n,m,t+1})$, as it is shown in Fig. 4(a). The corresponding part of the partition function includes five δ symbols, eight phases entering the function $\bar{T}_I(\bar{s}_t, \underline{s}_t)$ and two phases from the function $\bar{T}_K(\bar{s}_t, \bar{s}_{t+1}; \underline{s}_{t+1}, \underline{s}_t)$,

$$\Gamma = L^{-1} \sum_{s=1}^{L} e^{-i(g^*(\bar{s}_{n,m,t+1}, s) - g(\underline{s}_{n,m,t+1}, s))} \delta(\bar{s}_{n+1,m,t}, \underline{s}_{n+1,m,t}) \delta(\bar{s}_{n,m+1,t}, \underline{s}_{n,m+1,t}) \delta(\bar{s}_{n-1,m,t}, \underline{s}_{n-1,m,t}) \delta(\bar{s}_{n,m-1,t}, \underline{s}_{n,m-1,t})$$

$$\times e^{-i(f_v(s, \bar{s}_{n+1,m,t}) - f_v(s, \underline{s}_{n+1,m,t}))} e^{-i(f_v(\bar{s}_{n-1,m,t}, s) - f_v(\underline{s}_{n-1,m,t}, s))} e^{-i(f_h(s, \bar{s}_{n,m+1,t}) - f_h(s, \underline{s}_{n,m+1,t}))} e^{-i(f_h(\bar{s}_{n,m-1,t}, s) - f_h(\underline{s}_{n,m-1,t}, s))}. \quad (5.1)$$

Utilizing the unitarity of the kick evolution operator $u[g]$ [see Eq. (3.10)] and the properties of the Kronecker function the sum in Eq. (5.1) can be simplified to

$$\Gamma = \delta(\bar{s}_{n,m,t+1}, \underline{s}_{n,m,t+1}). \quad (5.2)$$

The contraction rules, conveniently, can be represented in a graphical form. In Fig. 4 they are shown as a transition from some initial configurations in the left column to the final configuration depicted in the right column in Fig. 4, where the "central" spin variables $(\bar{s}_{n,m,t+1}, \underline{s}_{n,m,t+1})$ has been eliminated according to the result Eq. (5.2). The contraction rule in Fig. 4(a) is formulated to act along the time direction. The contraction rule for the inverse direction $(t \to t - 1)$ is shown in Fig. 4(b).

Note also that similar contraction rules exist for the configurations with a reduced number of spin variables, see Fig. 4(c). In fact, a white ball (where a spin variable was eliminated in the previous steps) at some node (n, m, t) can be

replaced back by the identity multiplier presented as a sum of the Kronecker symbols, $1 \equiv L^{-1} \sum_{\bar{s}_{n,m,t}, \underline{s}_{n,m,t}=1}^{L} \delta(\bar{s}_{n,m,t}, \underline{s}_{n,m,t})$. This allows to extend the contraction rule for all combinations of balls including those, where some red balls are substituted by the white ones.

B. Application of the contraction rules

We now proceed with eliminating the spin variables from the partition function (4.18) by using the contraction rules graphically formulated in Fig. 4. Application of the contraction rules along the time axis, starting from $t = 0$ and continuing up to $t = T - 1$ allows us to eliminate most of the spin variables, resulting in the pyramidal structure shown in Fig. 5(a). The coordinates (n, m, t) of the remaining spin variables satisfy the equation $t + 1 \geqslant |n - 3/2| + |m - 3/2|$ [the positions of q_ℓ are fixed by Eqs. (4.7)]. Furthermore, the application of the contraction rule in the opposite time direction, i.e., t changes from T to 0, yields a parallelepiped-like structure shown in Fig. 5(b). This parallelepiped shrinks to a line when the operators $\mathbf{q}_\ell$ $(\ell = 5, 6, 7, 8)$ are positioned at one of the vertices of the pyramid base. If the operators $\mathbf{q}_\ell$ $(\ell = 5, 6, 7, 8)$ are placed outside the pyramid base, all spin variables can be eliminated by contraction rules and the resulting correlation function nullifies (for the traceless $\mathbf{q}_\ell$). Note that this observation is consistent with the causality argument given in Sec. II.

C. Dual-unitary case

Up to now we considered a general case, where no further systematic elimination of the spin variables can be done in the sum (4.18). Further progress in calculations becomes possible for the (partial) dual-unitary models. For definiteness, we choose the spatial direction marked by the index n to be dual with the time direction, i.e., the evolution operator $u[f_v]$ with the symbol f_v is unitary. The partial dual-unitarity assumption allows us to formulate the contraction rules for this spatial direction. Indeed, by using the unitarity of $u[f_v]$ the part of the sum (4.18),

$$\Gamma = L^{-1} \sum_{s=1}^{L} e^{-i(f_v(s, \bar{s}_{n+1,m,t}) - f_v(s, \underline{s}_{n+1,m,t}))}$$

$$\times \delta(\bar{s}_{n,m+1,t}, \underline{s}_{n,m+1,t}) \delta(\bar{s}_{n,m-1,t}, \underline{s}_{n,m-1,t})$$

$$\times \delta(\bar{s}_{n,m,t-1}, \underline{s}_{n,m,t-1}) \delta(\bar{s}_{n,m,t+1}, \underline{s}_{n,m,t+1})$$

$$\times e^{-i(f_h(s, \bar{s}_{n,m+1,t}) - f_h(s, \underline{s}_{n,m+1,t}))} e^{-i(f_h(\bar{s}_{n,m-1,t}, s) - f_h(\underline{s}_{n,m-1,t}, s))}$$

$$\times e^{-i(g(s, \bar{s}_{n,m,t+1}) - g(\underline{s}_{n,m,t+1}, s))} e^{-i(g(s, \bar{s}_{n,m,t-1}) - g(\underline{s}_{n,m,t-1}, s))} \quad (5.3)$$
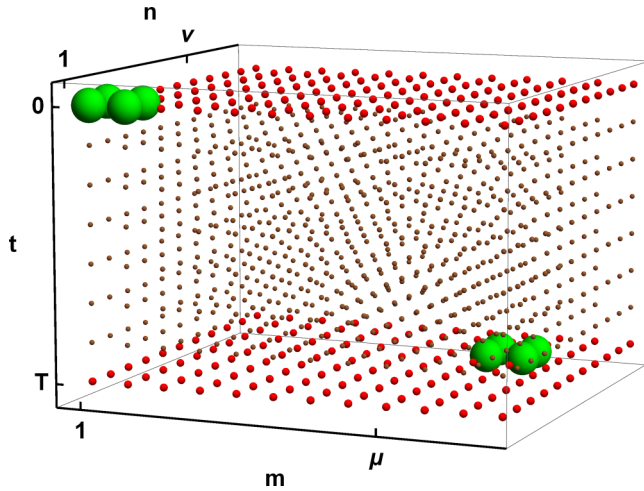

FIG. 3. 3D grid of the configuration space for calculation of the sum in Eq. (4.11) for the choice of $N = 11$, $M = 12$, $T = 7$, $\nu = 8$, and $\mu = 9$. The brown small balls correspond to the uncorrelated spin components, i.e., at the brown-ball vertex, say (n', m', t'), the summation over the spins $\bar{s}_{n',m',t'}$ and $\underline{s}_{n',m',t'}$ is performed independently. The red balls show the presence of the Kronecker symbol $\delta(\bar{s}_{n,m,t}, \underline{s}_{n,m,t})$ at the corresponding vertex (n, m, t) and the double summation reduces to a single sum over $\bar{s}_{n,m,t} = \underline{s}_{n,m,t} = 1, \dots, L$. The large green balls denote the positions of the matrices $\mathbf{q}_\ell$ entering the many-body operators $\bar{\Sigma}$ at $t = T$, and $\underline{\Sigma}$ at $t = 0$ [Eq. (4.7)]. The function $\bar{T}_I$ [Eq. (4.14)] defines the amplitudes of interaction between the balls in each time-plane, while $\bar{T}_K$ [Eq. (4.15)] is responsible for interaction between the time-planes.
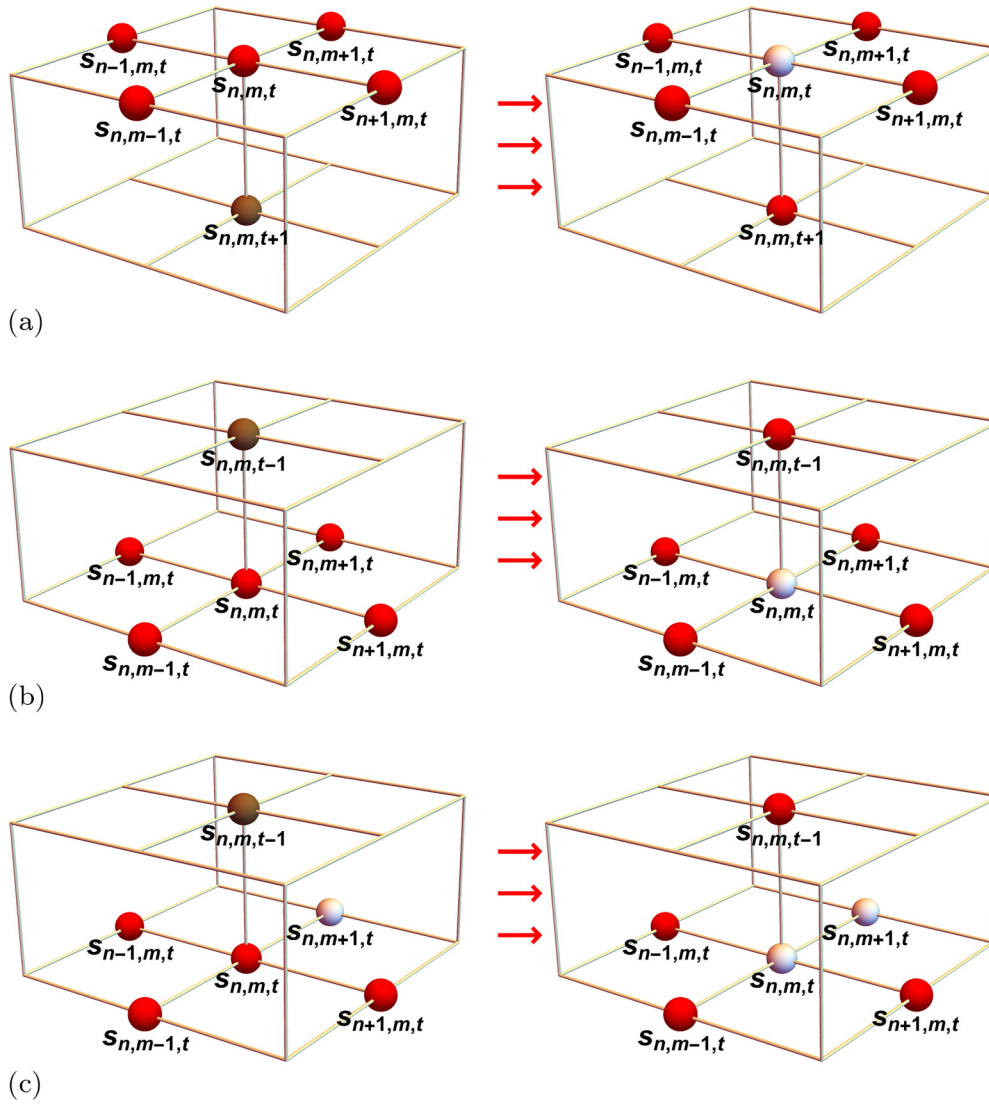
FIG. 4. The graphical representation of the contraction rules acting in time-direction (a) and in the inverse time-direction (b)(c). The pairs of spins $s_{n,m,t} \equiv (\bar{s}_{n,m,t}, \underline{s}_{n,m,t})$ are depicted by the balls of various colors. The summation over the correlated spins $\bar{s}_{n,m,t} = \underline{s}_{n,m,t} = 1, \ldots, L$ (the central red balls in the plots from the left column) surrounded by other correlated spins transforms the initially uncorrelated spins $\bar{s}_{n,m,t-1}$ and $\underline{s}_{n,m,t-1}$ (brown balls in the left column of the plots) into the delta-correlated ones (red balls in the corresponding positions $s_{n,m,t-1}$ in the right column). The white balls in the final configurations (right column of the plots) show the spins over which the summation has been performed. The diagram in (c) is a possible extension of the contraction rule for the case with a reduced number of spin variables.

simplifies to

$$\Gamma = \delta(\bar{s}_{n+1,m,t}, \underline{s}_{n+1,m,t}). \qquad (5.4)$$

This allows us to formulate the contraction rule in the dual (spatial) direction, which is illustrated by the diagram in Fig. 6(a). It can be naturally extended to the opposite direction of the same spatial axis, see Fig. 6(b).

Note here that the contraction rule in the spatial direction becomes useful only for $N > T + 2$. In this case, after subsequent applications of the contraction rules in the time direction, the border of the correlated spins is formed at some (at least one) given n. So that starting from this border we can subsequently apply the contraction rule in spatial direction.

Application of the contraction rules both in spatial and temporal directions yields trivial correlations for the majority of choices of the operators $\bar{\Sigma}$ and $\underline{\Sigma}$ in Eq. (4.7). All nontrivial cases result from a specific choice of $\mathbf{q}_\ell$ mutual positions. Namely, the operators $\mathbf{q}_\ell$ entering $\bar{\Sigma}$ and those from $\underline{\Sigma}$ have to be positioned along the line given by the equation $|n| = t$, $m = 0$. A number of possible realisations are analysed in Appendix B. As it is demonstrated there, for the operators $\bar{\Sigma}$, $\underline{\Sigma}$ with four-point supports, the nontrivial correlations arise only when $\mu = 0$, $\nu = T + 1$, see Eq. (4.7). An example of the spin structure resulting from the application of the contraction rules is depicted in Fig. 8(a) below.

Finally, if duality holds for both spatial directions (fully dual-unitary case), both $u[f_v]$ and $u[f_h]$ are unitary matrices.
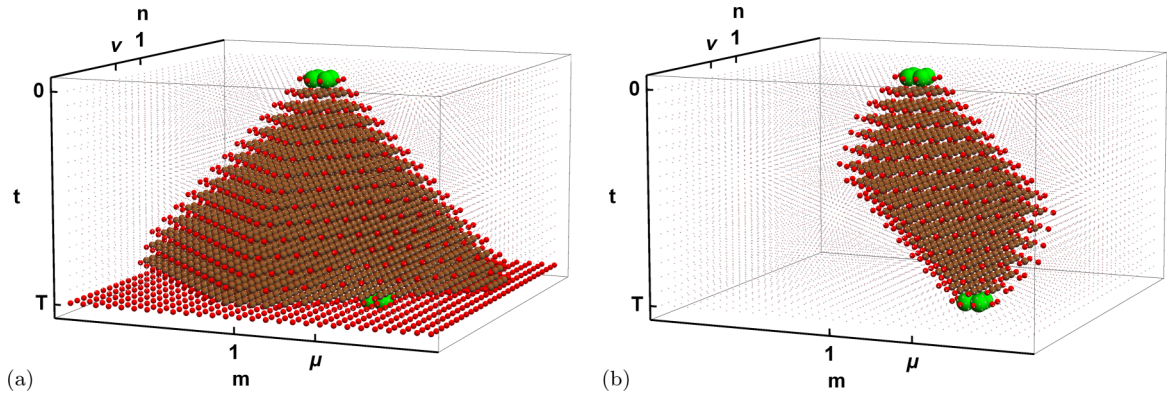
FIG. 5. (a) The spin configuration (parameters $N = M = 28$, $T = 15$, $\nu = 25$, and $\mu = 7$) obtained after consequent application of the contraction rule acting in the time direction [Fig. 4(a)] to the initial configuration (Fig. 3). The meaning of the ball's colors is the same as in the Fig. 4. For better visualisation, the spin array was periodically shifted along the horizontal and vertical axes and the white balls' radii were made small. (b) The spin configuration after the iterative application of the contraction rules acting in the inverse time-direction [Figs. 4(b) and 4(c)] to the structure given in the plot a, up to now, no duality was implied.

In this case, there is an additional set of contraction rules acting along the m axis. Applying contraction rules along the third axis leads to the elimination of all spin variables (for $T > 2$), regardless of the positions of $\bar{\Sigma}$ and $\underline{\Sigma}$. This implies that $C(T)$ vanishes entirely when $T > 2$.

To summarize this section, we list the general properties of the correlation function (4.11) established so far for two-dimensional lattice models: (i) For a general (nondual unitary) case the correlation function becomes trivial when the entries $\mathbf{q}_\ell$ ($\ell = 5, 6, 7, 8$) of the operator $\underline{\Sigma}$ are placed outside of the pyramid basis $|n - 3/2| + |m - 3/2| \leqslant t + 1$ (see Fig. 5). (ii) In the partially dual-unitary case, the correlation function becomes nontrivial when the operators $\bar{\Sigma}$ and $\underline{\Sigma}$ are aligned along the line $|n| = t$, $m = 0$ (see Appendix B). (iii) In the fully dual-unitary case at $T > 2$ the correlation function trivializes for any mutual positions of the operators $\mathbf{q}_\ell$.

VI. THE LOCAL CORRELATION FUNCTION AND THE TRANSFER OPERATOR

In this section, we show that similarly to the one-dimensional dual-unitary case, the correlation function $C(T)$ in a two-dimensional partially dual-unitary model can be expressed as an expectation value of the power of the low-dimension transfer operator [see Eq. (4.4)].

A. Operators with the two-point supports

Before addressing the correlation function for generic operators $\bar{\Sigma}$, $\underline{\Sigma}$ with four-point supports [see Eq. (4.7)], we illustrate our method for the case of the operators with the two-point supports. To this end we set in Eqs. (4.7) $\mathbf{q}_3 = \mathbf{q}_4 = \mathbf{q}_7 = \mathbf{q}_8 = \mathbb{1}$. An example of the structure of the uncorrelated spins obtained after applications of the contraction rules is illustrated in Fig. 7(a). In Appendix B we list all nontrivial
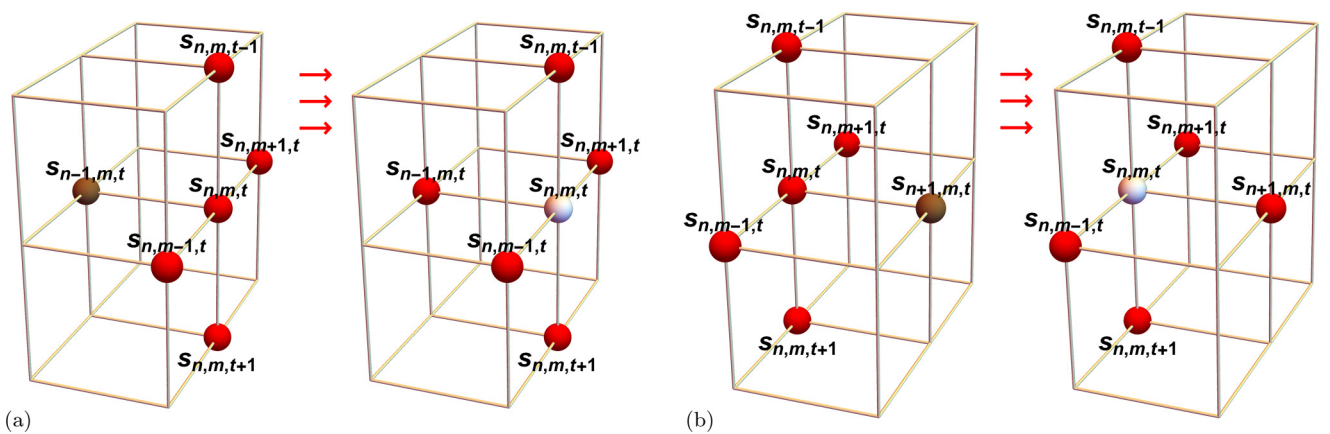
FIG. 6. The graphical representation of the contraction rules (a) in the spatial direction n, dual to the time direction, and (b) in the inverse direction. The summation over the correlated spins $\bar{s}_{n,m,t} = \underline{s}_{n,m,t}$ (the central red balls in the starting configurations) transforms the initially uncorrelated spins (brown balls) into the correlated ones (red balls in the final configurations). The white balls in the final configurations show the spins over which the summation has been performed. It is assumed that summation over the spin variables on the previous level (the spins $\bar{s}_{n-1,m,t}$ and $\underline{s}_{n-1,m,t}$ for the diagrams a, b and the spins $\bar{s}_{n+1,m,t}$ and $\underline{s}_{n+1,m,t}$ for the diagrams c, and d) has been made to generate a white/red ball at the corresponding position.
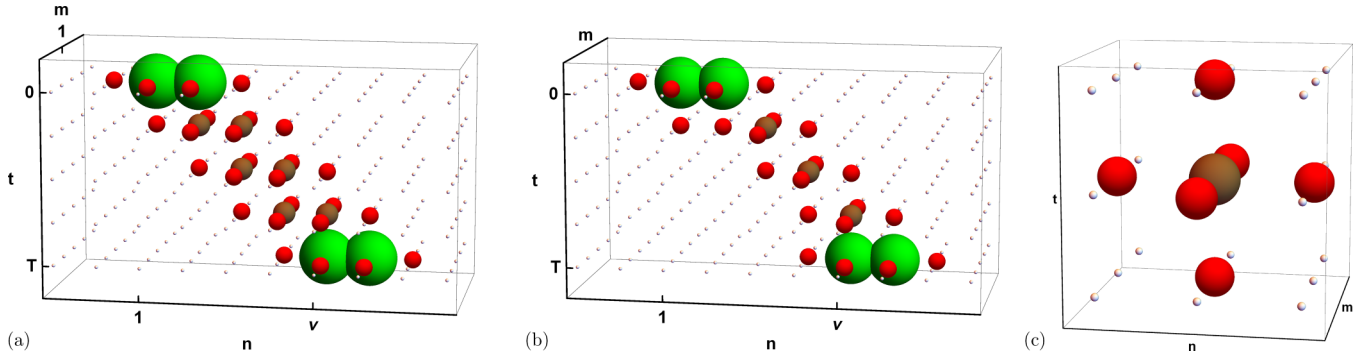
FIG. 7. (a) The spin structure obtained after application of the contraction rule to a partially dual-unitary map for $T = 4$, $M, N \gg T$ and $\mu = 1$, $\nu = T + 1$ in the case of operators with the two-point supports. (b) The spin structure that emerges after eliminating a part of the spin variables (see Appendix B for details). The horizontal coordinates n of the brown balls entering the intermediate linear structure of uncorrelated spins satisfy the equation $n = t + 2$ and are made up of the repeating blocks (unit cells). (c) The unit cell entering the spin-bridge structure corresponds to the transfer operator $\hat{T}$ [Eq. (6.5)].

structures obtained after applications of the contraction rules. A part of the spin variables can be, furthermore, eliminated from the corresponding partition functions (see Appendix B for more details), so that only one nontrivial structure (up to the mirror reflection with respect to the plane $n = const$) survive. It is shown in Fig. 7(b). The reduced locus of spins S' over which the summation still has to be performed (red, brown and green balls) is

$$S' = \{\, \bar{s}_{nmt} | (n, m, t) \in \mathcal{L}' \,\} \cup \{\, \underline{s}_{nmt} | (n, m, t) \in \mathcal{L}'' \,\} \tag{6.1}$$

with

$$\mathcal{L}' = \{(N, 1, 0), (1, M, 0), (1, 1, 0), (1, 2, 0), (2, M, 0), (2, 1, 0), (2, 2, 0), (3, 1, 0), (1, 1, 1), (T, 1, T),$$
$$(T + 1, M, T), (T + 1, 1, T), (T + 1, 2, T), (T + 2, M, T), (T + 2, 1, T), (T + 2, 2, T), (T + 3, 1, T)\}$$
$$\bigcup_{t=1}^{T-1} \{(t + 1, 1, t), (t + 2, 1, t), (t + 2, M, t), (t + 2, 2, t), (t + 3, 1, t)\}, \tag{6.2}$$

$$\mathcal{L}'' = \{\, (1, 1, 0), (2, 1, 0), (T + 1, 1, T), (T + 2, 1, T) \,\} \bigcup_{t=1}^{T-1} \{\, (t + 2, 1, t) \,\}. \tag{6.3}$$

This chain of spin variables is composed of repeating blocks shown in Fig. 7(c), with their centres positioned along the straight line $n = t$, $m = 0$. Since two neighboring unit cells are connected by a pair of spins, each block can be described by the $L^2 \times L^2$ transfer matrix $\hat{T}$ with the entries $\langle \chi, \eta | \hat{T} | \chi', \eta' \rangle$, where the indexes $\chi, \eta, \chi', \eta' = \overline{1, L}$ mark the values of the spins to be convoluted with the spins of the neighboring upper and lower unit cells. The matrix entries of $\hat{T}$ can be read off directly from the spin structure shown in Fig. 7(b), they are

$$\langle \chi, \eta | \hat{T} | \chi', \eta' \rangle = \frac{1}{L^5} \sum_{\bar{s}, \underline{s} = 1}^{L} \sum_{r_1, r_2 = 1}^{L} e^{-if_h(r_1, \bar{s}) + if_h(r_1, \underline{s})} e^{-if_h(\bar{s}, r_2) + if_h(\underline{s}, r_2)} e^{-if_v(\chi, \bar{s}) + if_v(\chi, \underline{s}) - ig(\bar{s}, \eta) + ig(\underline{s}, \eta)} e^{-if_v(\bar{s}, \eta') + if_v(\underline{s}, \eta') - ig(\chi', \bar{s}) + ig(\chi', \underline{s})}.$$
$$\tag{6.4}$$

The latter expression can be rewritten in a compact form

$$\langle \chi, \eta | \hat{T} | \chi', \eta' \rangle = \frac{1}{L^5} \sum_{r_1, r_2 = 1}^{L} \left| \sum_{s=1}^{L} e^{if_v(\chi, s) + ig(s, \eta) + if_v(s, \eta') + ig(\chi', s) + if_h(r_1, s) + if_h(s, r_2)} \right|^2, \tag{6.5}$$

The spin $\bar{s}$ and the conjugated spin $\underline{s}$ in this expression describe possible internal states of the central vertex in the unit cell (brown ball). The other two spin variables r_1 and r_2 describe the states of the neighboring lattice points in the horizontal direction (red balls). It is worth noting that the matrix entries $\langle \chi, \eta | T | \chi', \eta' \rangle$ coincide with those of the one-dimensional map [Eq. (4.5)] when we set the horizontal interactions f_h to zero.

The overall expression for the correlation function is given by the expectation value,

$$C(T) = \left\langle \bar{\Phi}_{\mathbf{q}_1, \mathbf{q}_2} \middle| \hat{T}^{T-2} \middle| \Phi_{\mathbf{q}_5, \mathbf{q}_6} \right\rangle, \tag{6.6}$$

where the entries of the transfer matrix $\hat{T}$ are given by Eq. (6.5) and the vectors $\langle\bar{\boldsymbol{\Phi}}_{\mathbf{q}_1,\mathbf{q}_2}|, |\boldsymbol{\Phi}_{\mathbf{q}_5,\mathbf{q}_6}\rangle$ are defined below by Eqs. (6.7)–(6.10).

The vector $|\bar{\boldsymbol{\Phi}}_{\mathbf{q}_1,\mathbf{q}_2}\rangle$ incorporates the function $\bar{\Phi}(\underline{s}_0,\bar{s}_0)$, function $\bar{T}_I(\bar{s}_0,\underline{s}_0)$ and a single phase drawn from the function $\bar{T}_K(\bar{s}_1,\bar{s}_1;\underline{s}_1,\underline{s}_0)$, so that

$$\langle\bar{\boldsymbol{\Phi}}_{\mathbf{q}_1,\mathbf{q}_2}|\chi,\eta\rangle = \frac{1}{L^5}\sum_{s_1,\bar{s}_2,\underline{s}_2=1}^{L}\bar{\Gamma}_{s_1}^{\bar{s}_2,\underline{s}_2}(\chi,\eta)\langle s_1|\mathbf{q}_1|s_1\rangle\langle\bar{s}_2|\mathbf{q}_2|\underline{s}_2\rangle \tag{6.7}$$

with the factor $\bar{\Gamma}_{s_1}^{\bar{s}_2,\underline{s}_2}(\chi,\eta)$ given by

$$\bar{\Gamma}_{s_1}^{\bar{s}_2,\underline{s}_2}(\chi,\eta) = e^{-ig(\chi,\bar{s}_2)+ig(\chi,\underline{s}_2)}e^{-if_v(s_1,\bar{s}_2)+if_v(s_1,\underline{s}_2)-if_v(\bar{s}_2,\eta)+if_v(\underline{s}_2,\eta)}\sum_{r_1,r_2=1}^{L}e^{-if_h(r_1,\bar{s}_2)+if_h(r_1,\underline{s}_2)-if_h(\bar{s}_2,r_2)+if_h(\underline{s}_2,r_2)}. \tag{6.8}$$

The vector $|\boldsymbol{\Phi}_{\mathbf{q}_5,\mathbf{q}_6}\rangle$ incorporates two time slices, namely it incorporates the functions $\Phi(\bar{s}_T,\underline{s}_T)$, $\bar{T}_I(\bar{s}_T,\underline{s}_T)$, $\bar{T}_K(\bar{s}_{T-1},\bar{s}_T;\underline{s}_T,\underline{s}_{T-1})$ and a single phase factor drawn from the function $\bar{T}_K(\bar{s}_{T-2},\bar{s}_{T-1};\underline{s}_{T-1},\underline{s}_{T-2})$. Note that the contraction rules were formulated in a symmetric manner, namely, we have introduced the additional matrices U_I into the functions $\Phi(\bar{s}_T,\underline{s}_T)$, so that the product $\Phi(\bar{s}_T,\underline{s}_T)\bar{T}_I(\bar{s}_T,\underline{s}_T)$ naturally simplifies to the scalar product $\langle\bar{s}_T|\Sigma|\underline{s}_T\rangle$. The entries $\langle\chi',\eta'|\bar{\boldsymbol{\Phi}}_{\mathbf{q}_5,\mathbf{q}_6}\rangle$ are defined by the expression

$$\langle\chi',\eta'|\boldsymbol{\Phi}_{\mathbf{q}_5,\mathbf{q}_6}\rangle = \frac{1}{L^5}\sum_{\bar{s}_1,\underline{s}_1,s_2=1}^{L}\Gamma_{\bar{s}_1,\underline{s}_1}^{s_2}(\chi',\eta')\langle\bar{s}_1|u^\dagger[g]\mathbf{q}_5 u[g]|\underline{s}_1\rangle\langle s_2|u^\dagger[g]\mathbf{q}_6 u[g]|s_2\rangle \tag{6.9}$$

with

$$\Gamma_{\bar{s}_1,\underline{s}_1}^{s_2}(\chi',\eta') = e^{-ig(\bar{s}_1,\eta')+ig(\underline{s}_1,\eta')}e^{-if_v(\chi',\bar{s}_1)+if_v(\chi',\underline{s}_1)-if_v(\bar{s}_1,s_2)+if_v(\underline{s}_1,s_2)}\sum_{r_1,r_2=1}^{L}e^{-if_h(r_1,\bar{s}_1)+if_h(r_1,\underline{s}_1)-if_h(\bar{s}_1,r_2)+if_h(\underline{s}_1,r_2)}. \tag{6.10}$$

The expression (6.6) was obtained for the structure shown in Fig. 7(a), when the spin-bridge structure is parallel to the line $n=t$. The correlation function

$$C(T) = \langle\bar{\boldsymbol{\Phi}}_{\mathbf{q}_1,\mathbf{q}_2}^r|\hat{\hat{T}}^{T-2}|\boldsymbol{\Phi}_{\mathbf{q}_5,\mathbf{q}_6}^r\rangle, \tag{6.11}$$

for the mirror-symmetric structure of spins (along the line $n=-t$) can be obtained by using the symmetry arguments. The "reflected" transfer matrix $\hat{\hat{T}}$ has the entries $\langle\eta',\chi'|\hat{\hat{T}}|\eta,\chi\rangle = \langle\eta',\eta|\hat{T}|\chi',\chi\rangle$ and the boundary vectors for the reflected picture are

$$\langle\eta,\chi|\bar{\boldsymbol{\Phi}}_{\mathbf{q}_1,\mathbf{q}_2}^r\rangle = \frac{1}{L^5}\sum_{\bar{s}_1,\underline{s}_1,s_2=1}^{L}\bar{\Gamma}_{\bar{s}_1,\underline{s}_1}^{s_2}(\eta,\chi)\langle\bar{s}_1|\mathbf{q}_1|\underline{s}_1\rangle\langle s_2|\mathbf{q}_2|s_2\rangle; \tag{6.12}$$

$$\langle\boldsymbol{\Phi}_{\mathbf{q}_5,\mathbf{q}_6}^r|\eta',\chi'\rangle = \frac{1}{L^5}\sum_{s_1,\bar{s}_2,\underline{s}_2=1}^{L}\Gamma_{s_1}^{\bar{s}_2,\underline{s}_2}(\eta',\chi')\langle s_1|u^\dagger[g]\mathbf{q}_5 u[g]|s_1\rangle\langle\bar{s}_2|u^\dagger[g]\mathbf{q}_6 u[g]|\underline{s}_2\rangle \tag{6.13}$$

with

$$\bar{\Gamma}_{\bar{s}_1,\underline{s}_1}^{s_2}(\eta,\chi) = e^{-ig(\chi,\bar{s}_1)+ig(\chi,\underline{s}_1)}e^{-if_v(\bar{s}_1,s_2)+if_v(\underline{s}_1,s_2)-if_v(\eta,\bar{s}_1)+if_v(\eta,\underline{s}_1)}\sum_{r_1,r_2=1}^{L}e^{-if_h(r_1,\bar{s}_1)+if_h(r_1,\underline{s}_1)-if_h(\bar{s}_1,r_2)+if_h(\underline{s}_1,r_2)}, \tag{6.14}$$

$$\Gamma_{s_1}^{\bar{s}_2,\underline{s}_2}(\eta',\chi') = e^{-ig(\bar{s}_2,\eta')+ig(\underline{s}_2,\eta')}e^{-if_v(\bar{s}_2,\chi')+if_v(\underline{s}_2,\chi')-if_v(s_1,\bar{s}_2)+if_v(s_1,\underline{s}_2)}\sum_{r_1,r_2=1}^{L}e^{-if_h(r_1,\bar{s}_2)+if_h(r_1,\underline{s}_2)-if_h(\bar{s}_2,r_2)+if_h(\underline{s}_2,r_2)}. \tag{6.15}$$

The more general case of four-point support boundary operators is considered in the next section.

B. Operators with the four-point supports

For generic operators $\bar{\Sigma}$, $\underline{\Sigma}$ with four-point supports [see Eq. (4.7)], the spin structure emerging after the application of the contraction rules gets the structure shown in Fig. 8(b). Each unit cell [Fig. 8(c)] composing the bridge between the boundaries (green balls) is described now by the $L^4 \times L^4$ transfer matrix $\hat{T}$ with the entries

$$\langle\chi,\eta,\chi_1,\eta_1|\hat{T}|\chi',\eta',\chi_1',\eta_1'\rangle$$

$$= \frac{1}{L^7}\sum_{r_1,r_2=1}^{L}\left|\sum_{s_1,s_2=1}^{L}e^{if_v(\chi,s_1)+ig(s_1,\eta)+if_v(s_1,\eta')+ig(\chi',s_1)}e^{if_h(r_1,s_1)+if_h(s_1,s_2)+if_h(s_2,r_2)}e^{if_v(\chi_1,s_2)+ig(s_2,\eta_1)+if_v(s_2,\eta_1')+ig(\chi_1',s_2)}\right|^2. \tag{6.16}$$
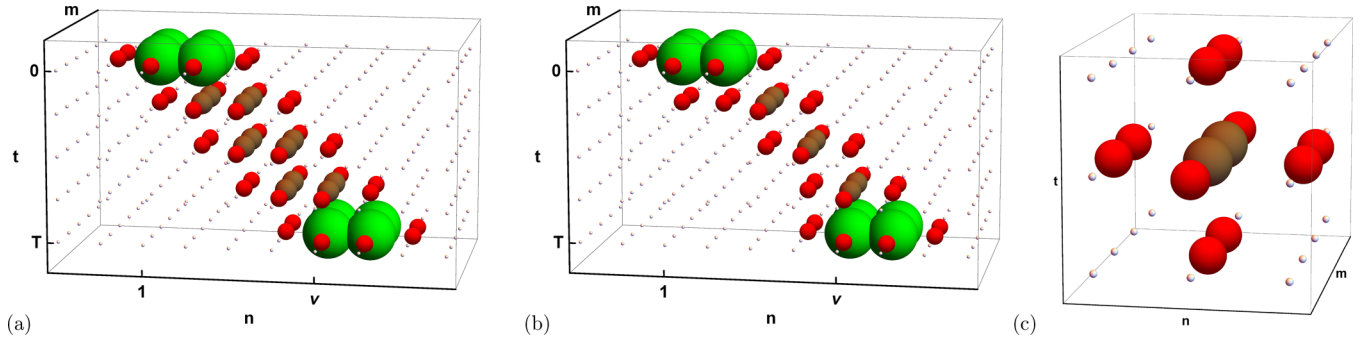
FIG. 8. (a) The structure of spins obtained after application of the contraction rule to a partially dual-unitary map for $T = 4$, $M, N \gg T$ and $\mu = 1$, $\nu = T + 1$ corresponding to the nontrivial correlation function $C(T)$. (b) The spin structure obtained from the one in (a) being reduced by taking into account the boundary conditions (see Appendix B for details). (c) The unit cell entering the linear structure of spins corresponds to the transfer operator $\hat{T}$ [Eq. (6.16)].

Note that after summation over the indexes χ_1, η_1, the matrix element $\langle \chi, \eta, \chi_1, \eta_1 | \hat{T} | \chi', \eta', \chi_1', \eta_1' \rangle$ reduces to the one in Eq. (6.5). As in the case of the operators with two-point supports, the correlation function is given by the expectation value,

$$C(T) = \langle \bar{\boldsymbol{\Phi}}_{\bar{\Sigma}} | \hat{T}^{T-2} | \boldsymbol{\Phi}_{\underline{\Sigma}} \rangle, \qquad (6.17)$$

with the vectors $\langle \bar{\boldsymbol{\Phi}}_{\bar{\Sigma}} |$, $| \boldsymbol{\Phi}_{\underline{\Sigma}} \rangle$ determined by the operators $\mathbf{q}_1$, $\mathbf{q}_2$, $\mathbf{q}_3$, $\mathbf{q}_4$ and $\mathbf{q}_5$, $\mathbf{q}_6$, $\mathbf{q}_7$, $\mathbf{q}_8$, respectively. The explicit expressions for these vectors are quite cumbersome, and we do not provide them here.

C. Spectral properties of the transfer operator

It follows immediately from the unitarity of matrices $u[g]$ and $u[f_v]$ that the transfer matrix (6.16), as well as its reduced form (6.16), is doubly stochastic, i.e., it satisfies the property

$$\sum_{\chi_1, \eta_1, \chi, \eta = 1}^{L} \langle \chi, \eta, \chi_1, \eta_1 | \hat{T} | \chi', \eta', \chi_1', \eta_1' \rangle = 1,$$

$$\sum_{\chi_1', \eta_1', \chi', \eta' = 1}^{L} \langle \chi, \eta, \chi_1, \eta_1 | \hat{T} | \chi', \eta', \chi_1', \eta_1' \rangle = 1. \qquad (6.18)$$

The identity (6.18), in particular, means that the spectrum of $\hat{T}$ is contained within the unit disk on the complex plane with the largest eigenvalue $\lambda_0 = 1$. The eigenvector corresponding to the maximal eigenvalue has the constant entries,

$$\langle \mathcal{E} | \chi, \eta, \chi_1, \eta_1 \rangle = 1, \quad \chi, \eta, \chi_1, \eta_1 \in \overline{1, L}.$$

It is straightforward to see that for traceless operators $\bar{\Sigma}$, $\underline{\Sigma}$ both $\langle \bar{\boldsymbol{\Phi}}_{\bar{\Sigma}} |$ and $| \boldsymbol{\Phi}_{\underline{\Sigma}} \rangle$ are orthogonal to $\mathcal{E}$,

$$\langle \bar{\boldsymbol{\Phi}}_{\bar{\Sigma}} | \mathcal{E} \rangle = \langle \mathcal{E} | \boldsymbol{\Phi}_{\underline{\Sigma}} \rangle = 0.$$

As a result, for the traceless operators, the leading contribution into the correlation function (6.17) and (6.6) is determined by the second largest eigenvalue, λ_1 ($|\lambda_1| < |\lambda_0|$), of the operator $\hat{T}$. Thus, generically, the nontrivial part of the correlation function decays exponentially with time and the characteristic decay rate is $| \ln |\lambda_1| |^{-1}$. It is instructive, therefore, to study the dependence of λ_1 on the internal parameters of the model. In

the next section, we provide an analysis of the transfer matrix spectrum for a particular choice of the map.

VII. APPLICATIONS

In this section, we illustrate our results using two particular realizations of the general model: coupled cat maps and kicked Ising spin-lattice. Specifically, we provide a detailed spectral analysis of the transfer matrix (6.5), for the case of operators with two-point supports.

A. Coupled cat maps

One of the best studied and understood examples of systems with chaotic dynamics is provided by Arnold's cat map, which is the hyperbolic automorphism of the two-dimensional unit torus [44]. The cat map acts in the 2D phase space: $\{x_t, p_t\} \rightarrow \{x_{t+1}, p_{t+1}\}$, with x_t, p_t being the coordinate and momentum at the discrete moment of time t. The generation function of a single perturbed cat map is the function

$$\mathcal{S}(x_t, x_{t+1}) = \tfrac{1}{2}\left(a x_t^2 + 2c x_t x_{t+1} + b x_{t+1}^2\right) + \mathcal{V}(x_t), \qquad (7.1)$$

where a, b, c are integers and $\mathcal{V}(x)$ is an arbitrary smooth real-valued function satisfying the periodic conditions, $\mathcal{V}(x + 1) = \mathcal{V}(x)$. The equations of motion are defined through the derivatives of the action, $x_t = \partial \mathcal{S} / \partial x_{t+1}$, $p_t = -\partial \mathcal{S} / \partial x_t$. Their explicit form is

$$x_{t+1} = a x_t + p_t + \mathcal{V}'(x_t), \qquad \mathrm{mod}\ 1,$$
$$p_{t+1} = (ab - 1) x_t + b p_t, \qquad \mathrm{mod}\ 1, \qquad (7.2)$$

where we set $c = -1$ for the sake of simplicity of exposition. The regime of fully chaotic dynamics is achieved when $a + b > 2$. The above dynamical equations can be cast into a more compact, Newton form

$$x_{t-1} + x_{t+1} = (a + b) x_t + \mathcal{V}'(x_t) \quad \mathrm{mod}\ 1. \qquad (7.3)$$

An extension of the cat map to the many-body setting, *coupled cat map lattice*, was introduced in [4] and subsequently studied in a number of papers [5–7] both on classical and quantum levels. In this model, $\mathcal{N}$ cat maps, placed on the sites of the D-dimensional lattice $\mathbb{Z}^D$, are coupled with the help of nearest-neighbor linear interactions. The resulting dynamical

equations for $D = 2$ take the form

$$d_h(x_{n+1,m,t} + x_{n-1,m,t}) + d_v(x_{n,m+1,t} + x_{n,m-1,t})$$
$$= x_{n,m,t+1} + x_{n,m,t-1} - (a+b)x_{n,m,t} - \mathcal{V}'(x_{n,m,t}) \quad \mod 1, \tag{7.4}$$

where $x_{n,m,t}$ stands for the cat's coordinate at the (n, m)-site of the lattice. The constants d_h, d_v in Eq. (7.4) determine the strength of the coupling in the horizontal and vertical directions, respectively. The model is partially dual unitary if one of the coupling constants equals -1 and fully dual unitary when $d_h = d_v = -1$. Indeed, as can be readily observed, the Eq. (7.4) remains invariant under the exchange of t and n if $d_h = -1$, or under the exchange of t and m if $d_v = -1$. Since we are primarily interested in the partially dual-unitary case, we fix $d_v = -1$ from now on and leave d_h as a free parameter.

The quantization of a single cat map can be carried out according to a general procedure for quantization of a linear automorphism, see [45,46]. The corresponding unitary time evolution is given by $L \times L$ matrix $u[g]$ of the form (3.7),

where the function g is determined by the classical action (7.1) at $c = -1$, according to the agreement we made in Eq. (7.2),

$$g(s, s') = \frac{2\pi}{L} \mathcal{S}(s, s'). \tag{7.5}$$

Note that $u[g]$ is a Hadamard matrix, with the factor $2\pi/L$ playing the role of the effective Planck's constant. An extension of this quantization procedure to coupled cat map lattice was presented in [7]. In accordance with the structure of the classical map, the corresponding quantum evolution can be split into the product, $U = U_K[g]U_I[f_h, f_v]$, where U_K is given by the tensor product of $\mathcal{N}$ operators $u[g]$ and $U_I[f_h, f_v]$ is an interaction part provided by the diagonal matrix (3.6), with

$$f_v(s, s') = \frac{2\pi}{L} ss', \quad f_h(s, s') = \frac{2\pi}{L} d_h ss'. \tag{7.6}$$

Since the resulting time evolution U is partially dual unitary and possesses the required form (3.2), we can straightforwardly apply the results from Sec. VI. For the above set of functions g, f_v, f_h the transfer matrix entries [Eq. (6.5)] become

$$\langle \chi, \eta | \hat{\boldsymbol{T}} | \chi', \eta' \rangle = \frac{1}{L^5} \sum_{r_1,r_2=1}^{L} \left| \sum_{s=1}^{L} e^{i\frac{2\pi}{L}s(\chi-\eta+\eta'-\chi')+i\frac{\pi}{L}(a+b)s^2+i\mathcal{V}(s/L)+i\frac{2\pi}{L}d_h s(r_1+r_2)} \right|^2. \tag{7.7}$$

A brief analysis of the matrix elements [Eq. (7.7)] immediately shows that, since the matrix indexes enter in the combination $(\chi - \eta) - (\chi' - \eta')$, among all L^2 matrix rows only L rows are linearly independent [see Fig. 12(a) below]. Therefore, for each choice of L the transfer matrix has only L nonzero eigenvalues. The nontrivial kernel of the transfer matrix is the Toeplitz matrix, i.e., the matrix entries depend on the difference of their indexes. It has the entries K_{j-k} $(j, k = \overline{0, L-1})$, with

$$K_j = \frac{1}{L^5} \sum_{r_1,r_2=1}^{L} \left| \sum_{s=1}^{L} e^{i\frac{2\pi}{L}sj+i\frac{\pi}{L}(a+b)s^2+i\mathcal{V}(s)+i\frac{2\pi}{L}d_h s(r_1+r_2)} \right|^2. \tag{7.8}$$

The Toeplitz matrices are known to be diagonalizable by the Fourier matrix with the entries $F_{k,\ell} = L^{-1/2} \exp[2\pi i k\ell/L]$, namely

$$\sum_{j,k=0}^{L-1} F_{\ell,j}^* K_{j-k} F_{k,\ell'} = \delta(\ell - \ell')\lambda_\ell, \tag{7.9}$$

$$\lambda_\ell = \sum_{j=0}^{L-1} e^{-i\frac{2\pi}{L}\ell j} K_j, \tag{7.10}$$

where ℓ runs from 0 to $L - 1$. After performing the summation in Eq. (7.10), the nontrivial eigenvalues λ_ℓ of T can be written

in a compact form

$$\lambda_\ell = \bar{\lambda}_\ell e^{i\frac{\pi\ell}{L}[(a+b)\ell+2(L+1)d_h]} R_{L,\ell}(d_h), \tag{7.11}$$

$$R_{L,\ell}(d_h) = \frac{\sin^2 \pi d_h \ell}{L^2 \sin^2 \frac{\pi d_h \ell}{L}}, \tag{7.12}$$

where the first factor

$$\bar{\lambda}_\ell = \frac{1}{L} \sum_{s=1}^{L} e^{i\frac{2\pi}{L}(a+b)s\ell+i\mathcal{V}(s/L)-i\mathcal{V}(s/L+\ell/L)}, \tag{7.13}$$

represents eigenvalues of the transfer matrix for the dual-unitary couple cat map chain ($D = 1$). The real and the imaginary parts, as well as the absolute value of $\bar{\lambda}_\ell$, are plotted in Fig. 9 for $L = 27$ and the perturbation $\mathcal{V}(s) = \cos 2\pi s$. The plot showing dependence of $\bar{\lambda}_\ell$ on L is given in Fig. 10.

As expected, at $\ell = 0$, the leading eigenvalue is $\lambda_0 = 1$, independently of the model's parameters. For all other eigenvalues we have $|\lambda_\ell| \leqslant |\bar{\lambda}_\ell| \leqslant 1$ due to the presence of the modulating function $R_{L,\ell}(d_h)$, bounded from above and below, $0 \leqslant R_{L,\ell}(d_h) \leqslant 1$. At $d_h = 0$ the modulating function equals 1 identically, which returns us to the one-dimensional cat map chain. For $d_h = -1$ corresponding to the fully dual-unitary case, the function $R_{L,\ell}(d_h)$ equals zero identically for $\ell > 0$. From this observation, it follows that the correlation function $C(t)$ vanishes for the traceless observables, as it should be for a fully dual-unitary model. Moreover, the function $R_{L,\ell}(d_h)$ and the correlation function $C(t)$ equal zero for almost all other integer values of d_h. Exceptions occur in cases where L is a product of several prime numbers, for example,
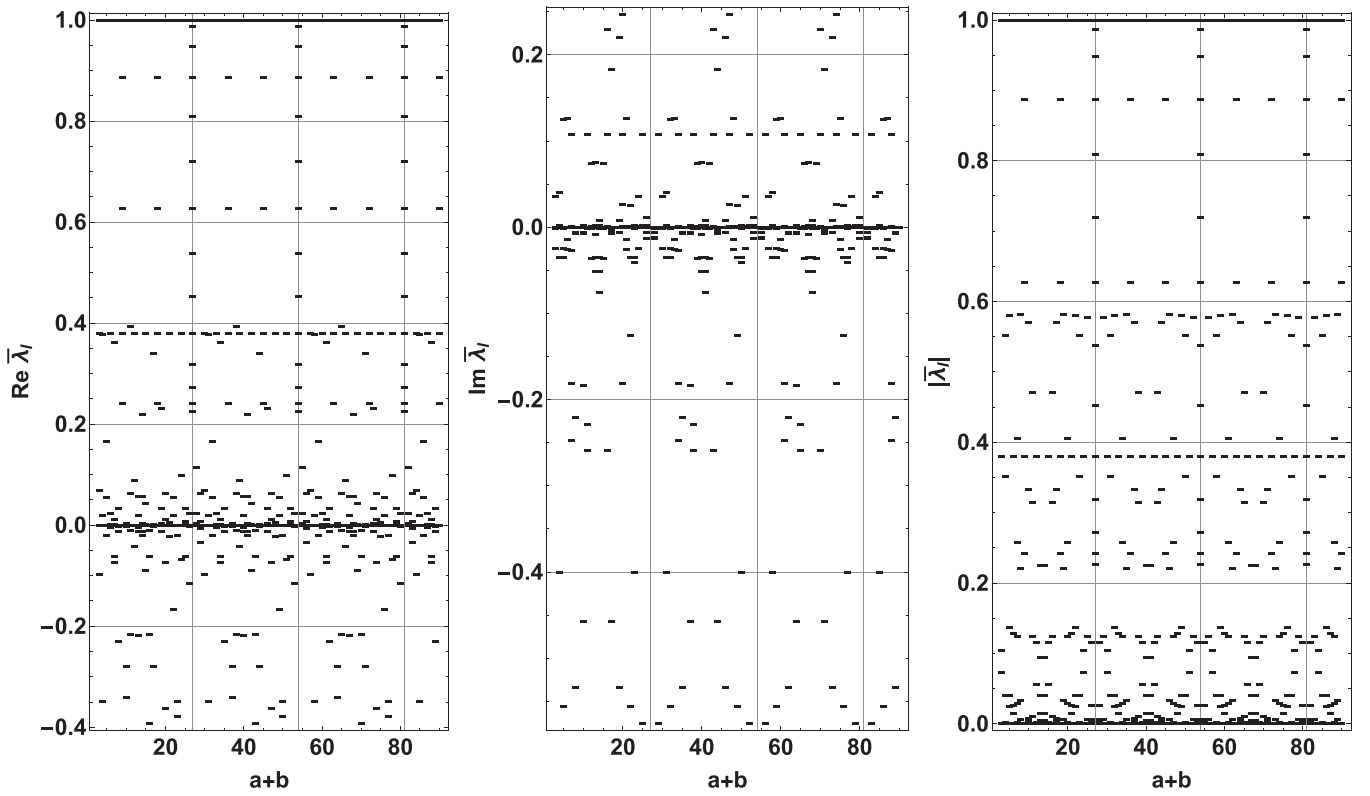
FIG. 9. Real part, imaginary part, and the absolute value of the eigenvalues $\bar{\lambda}_\ell$ [Eq. (7.13)] vs $a + b$ at $L = 27$ and $\mathcal{V}(s) = \cos 2\pi s$. The eigenvalues change periodically with respect to $a + b$ with the period L.
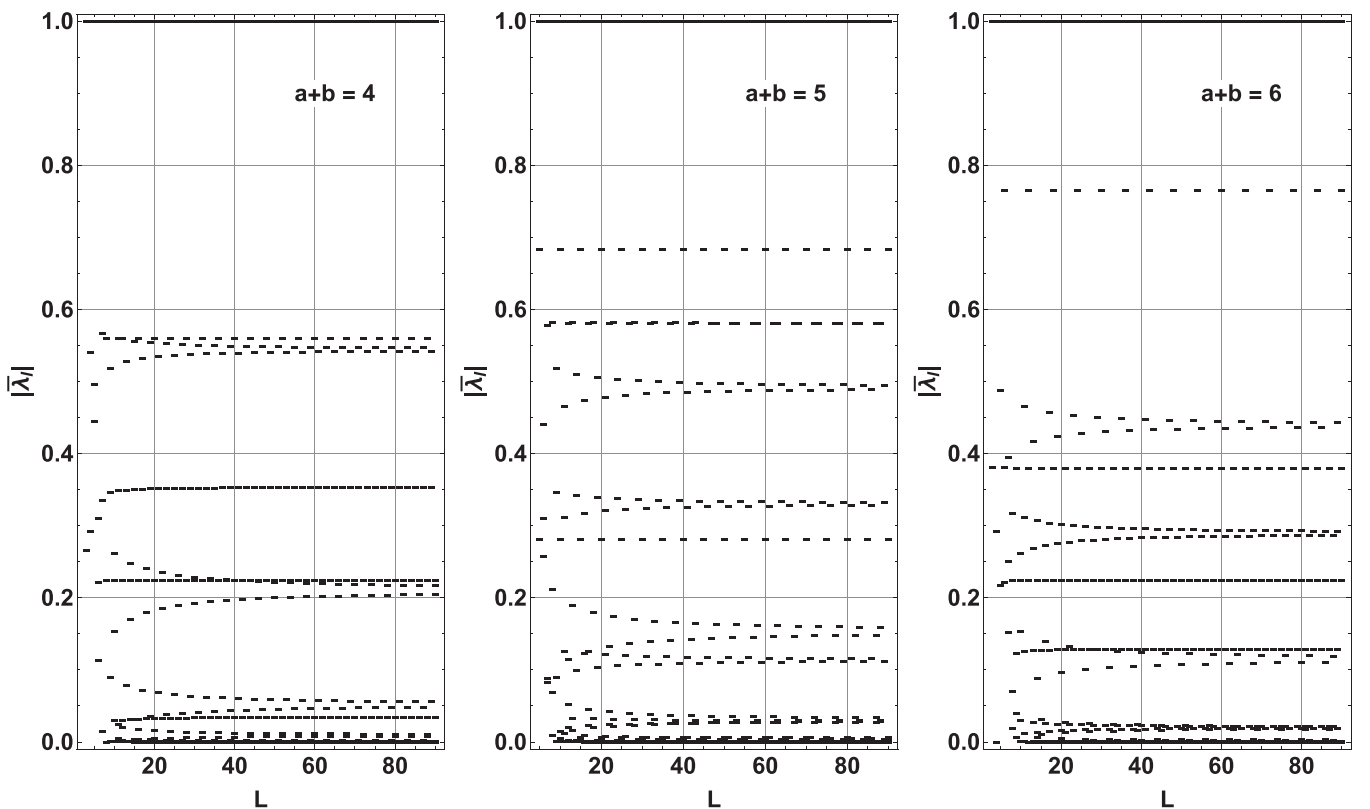

FIG. 10. The spectrum $|\bar{\lambda}_\ell|$ [Eq. (7.13)] of the one-dimensional cat map model transition operator plotted with respect to the particle Hilbert space dimension L for three different values of the parameter $a + b$. The perturbation is chose to be $\mathcal{V}(s) = \cos 2\pi s$.
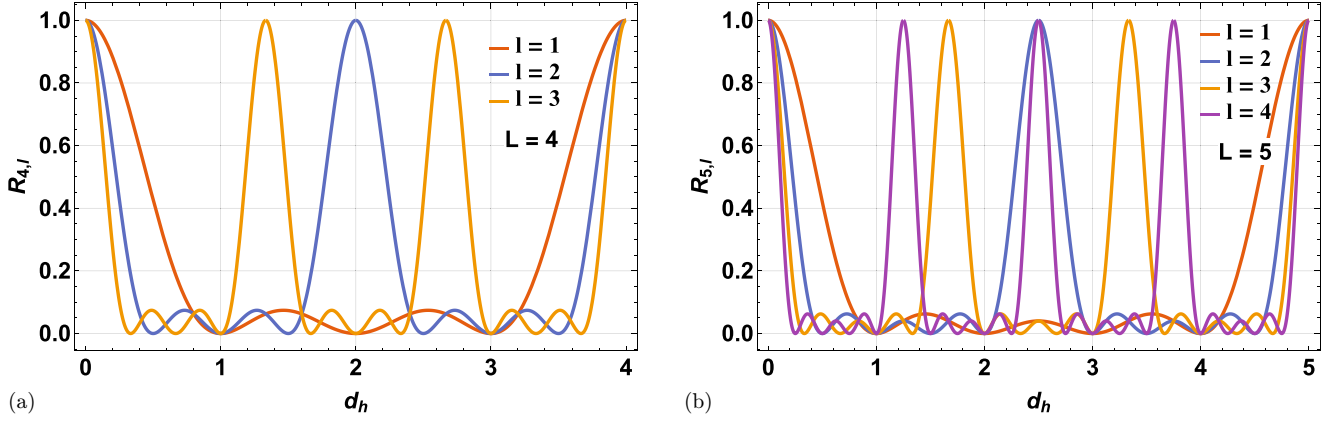
FIG. 11. The eigenvalue modulation function (a) $R_{4,\ell}(d_h)$ and (b) $R_{5,\ell}(d_h)$ plotted vs d_h for $\ell > 0$ [Eq. (7.11)]. Only the single period of each function is plotted.

$L = p_1 p_2$ and $p_1, p_2 \neq 1$. Here, the function $R_{L,\ell}(d_h)$ can attain its maximum value of 1 at certain values of d_h other than 0. For instance $R_{L=p_1 p_2, \ell=p_1}(p_2) = R_{L=p_1 p_2, \ell=p_2}(p_1) = 1$. To demonstrate this features we plotted the functions $R_{L=4,\ell}(d_h)$, and $R_{L=4,\ell}(d_h)$ in Fig. 11.

B. The kicked Ising spin lattice

In this part, we illustrate our results on the particular example of the minimal dimension model ($L = 2$), the kicked Ising spin-1/2 lattice. This model is known to have the dual-unitary regime and has served as a paradigm in the field of many-body quantum chaos, see [8–11,47]. Although the model has primarily been investigated in one dimension ($D = 1$), its extension to many-dimensional ($D > 1$) lattices is straightforward [48]. The system evolution is governed by the Hamiltonians

$$H_I = \sum_{n=1}^{N} \sum_{m=1}^{M} d_v \hat{\sigma}_{n,m}^z \hat{\sigma}_{n+1,m}^z + d_h \hat{\sigma}_{n,m}^z \hat{\sigma}_{n,m+1}^z + h \hat{\sigma}_{n,m}^z,$$

$$H_K = \sum_{n=1}^{N} \sum_{m=1}^{M} J \hat{\sigma}_{n,m}^x, \tag{7.14}$$

where the operators $\hat{\sigma}_{n,m}^\alpha$ are the Pauli matrices with $\alpha = x, y, z$ (see Appendix C), acting in the two-dimensional Hilbert space ($L = 2$) of a single spinor with the lattice index (m, n). As everywhere above, we assume that $n = \overline{1, N}, m = \overline{1, M}$ as well as the cyclic boundary conditions, i.e., $\hat{\sigma}_{N+1,m}^\alpha \equiv \hat{\sigma}_{1,m}^\alpha$, $\hat{\sigma}_{n,M+1}^\alpha \equiv \hat{\sigma}_{n,1}^\alpha$. To make the model partially dual unitary we set $J = \pi/2, d_v = \pi/4$. With this choice the matrix $u[g]$ has

the form

$$u[g] = \frac{1}{\sqrt{2}} \begin{pmatrix} 1 & -i \\ -i & 1 \end{pmatrix}, \tag{7.15}$$

while the matrices $u[f_{v/h}]$ are given by

$$u[f_{v/h}] = \frac{1}{\sqrt{2}} \begin{pmatrix} e^{-i(d_{v/h}+h_{v/h})} & e^{id_{v/h}} \\ e^{id_{v/h}} & e^{-i(d_{v/h}-h_{v/h})} \end{pmatrix}, \tag{7.16}$$

where $h_h = h, h_v = 0$. The function $g(s, s') = \frac{\pi}{4}((2s - 3)(2s' - 3) - 1)$ and $f_{v/h}(s, s') = d_{v/h}(2s - 3)(2s' - 3) + h_{v/h}(s + s' - 3)$. Note that the matrices $u[f_v]$ and $u[g]$ are Hadamard matrices, at the choice $J = \pi/2, d_v = \pi/4$ they coincide up to the constant phase factor $e^{i\pi/4}$, which is irrelevant as far as the correlation function is concerned. In accordance with the Eq. (6.5), the resulting 4×4 transfer matrix $\langle \chi, \eta | \hat{T} | \chi', \eta' \rangle$ in the basis $\{|1, 1\rangle, |2, 2\rangle, |1, 2\rangle, |2, 1\rangle\}$ has the 2×2 block structure

$$\hat{T} = \begin{pmatrix} \alpha E & \beta E \\ \beta E & \alpha E \end{pmatrix},$$

$$\alpha = \frac{1}{4}(1 + \cos^2 2d_h \cos 2h), \quad \beta = \frac{1}{4}(1 - \cos^2 2d_h \cos 2h), \tag{7.17}$$

where E is the 2×2 matrix with the unit entries, i.e., $E_{i,j} = 1$ for all i, j. The transfer matrix has two zero eigenvalues, the eigenvalue $\lambda_0 = 1$ with the eigenvector $\frac{1}{2}(1, 1, 1, 1)$ and the eigenvalue

$$\lambda_1 = \cos^2 2d_h \cos 2h, \tag{7.18}$$

with the corresponding eigenvector $\frac{1}{2}(-1, -1, 1, 1)$.

By using the spectrum of $\hat{T}$, the correlation function $C(T)$ for the traceless operators $\mathbf{q}_i$ takes the form

$$C(T) = -\frac{1}{2} \lambda_1^{T-2} \cos^4 2d_h \langle 1|u^\dagger[g]\mathbf{q}_6 u[g]|1\rangle [\cos 2h(\langle 1|u^\dagger[g]\mathbf{q}_5 u[g]|2\rangle - \langle 2|u^\dagger[g]\mathbf{q}_5 u[g]|1\rangle) + i \sin 2h(\langle 1|u^\dagger[g]\mathbf{q}_5 u[g]|2\rangle$$

$$+ \langle 2|u^\dagger[g]\mathbf{q}_5 u[g]|1\rangle)][\cos 2h(\langle 1|\mathbf{q}_2|2\rangle - \langle 2|\mathbf{q}_2|1\rangle) + i \sin 2h(\langle 1|\mathbf{q}_2|2\rangle + \langle 2|\mathbf{q}_2|1\rangle)]\langle 1|\mathbf{q}_1|1\rangle. \tag{7.19}$$

It is instructive to calculate the correlation function for the operators $\mathbf{q}_\ell$ taken from the set of Pauli matrices. Obviously, only the choices $\mathbf{q}_1 = \hat{\sigma}^z, \mathbf{q}_6 = \hat{\sigma}^y$, and $\mathbf{q}_2 = \hat{\sigma}^x, \hat{\sigma}^y, \mathbf{q}_5 = \hat{\sigma}^x, \hat{\sigma}^z$ correspond to the nonzero correlation function. In total there are four combinations, which lead to a nontrivial correlation function. The results of calculations are gathered in Appendix C.
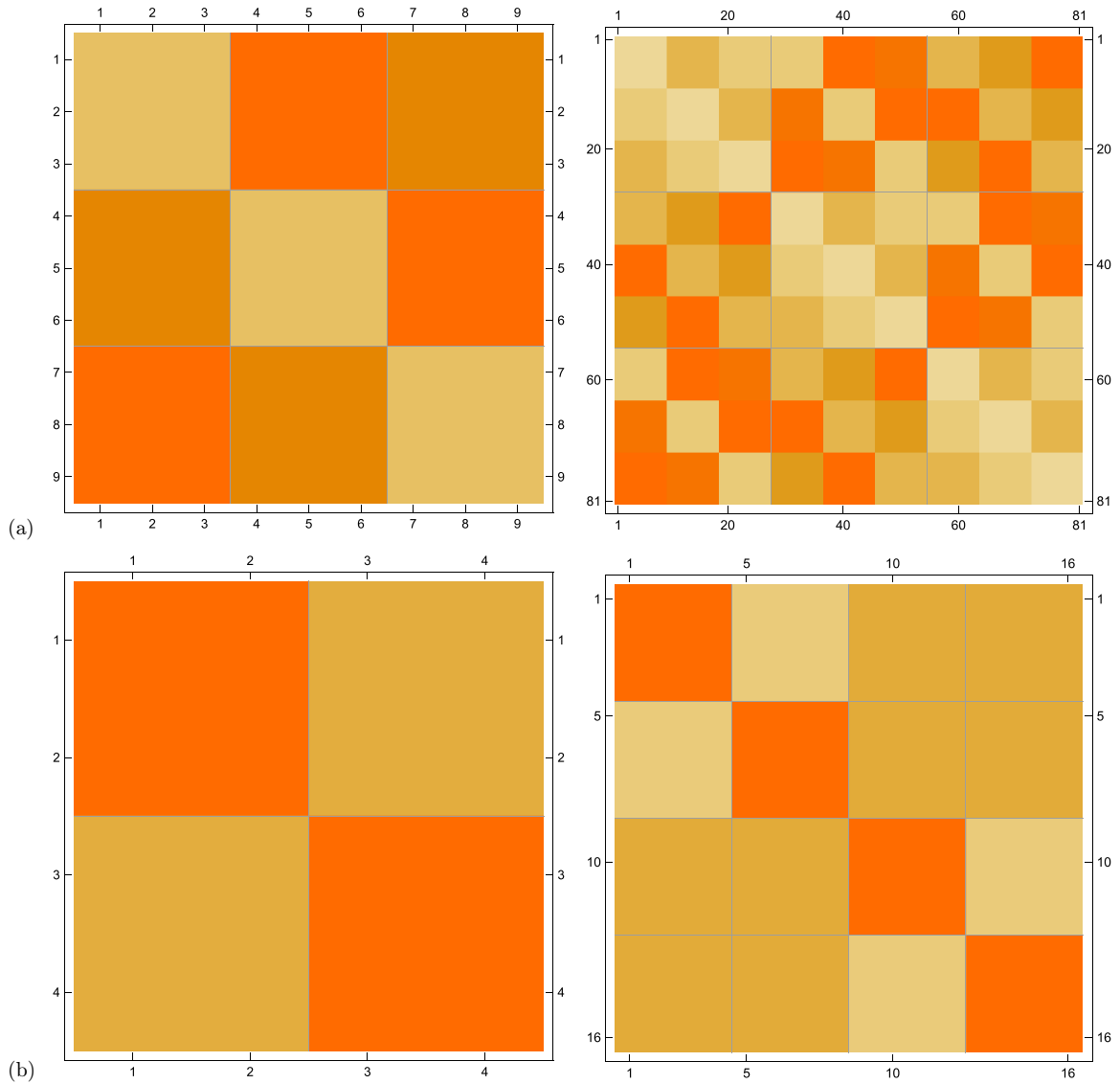
FIG. 12. The typical block structures of transfer matrices $\hat{T}$ for (a) the coupled cat map model at $L = 3$, and (b) for the kicked Ising spin lattice. The identical colors (arbitrary choice for each case) correspond to the identical matrix elements. The first column contains the plots for the four-point transfer matrices [Eqs. (6.5), (7.7), and (7.17)], and in the second column the pictures of the eight-point transfer [Eqs. (6.16) and (7.20)] matrices are gathered.

Finally, consider the transfer matrix [Eq. (6.16)] for the correlation function of four-point supported operators for the kicked Ising spin lattice model. The matrix $\langle \chi, \eta, \chi_1, \eta_1 | \hat{T} | \chi', \eta', \chi'_1, \eta'_1 \rangle$ can be written in a block-hierarchical structured form [see Fig. 12(b)]

$$\hat{T} = \begin{pmatrix} \tilde{\alpha}E & \breve{\beta}E & \tilde{\gamma}E & \tilde{\gamma}E \\ \breve{\beta}E & \tilde{\alpha}E & \tilde{\gamma}E & \tilde{\gamma}E \\ \tilde{\gamma}E & \tilde{\gamma}E & \tilde{\alpha}E & \breve{\beta}E \\ \tilde{\gamma}E & \tilde{\gamma}E & \breve{\beta}E & \tilde{\alpha}E \end{pmatrix}, \qquad (7.20)$$

where

$$\tilde{\alpha} = \tfrac{1}{8}(4\cos^4 h \cos^2 2d_h + \sin^2 2d_h),$$

$$\tilde{\beta} = \tfrac{1}{8}(4\sin^4 h \cos^2 2d_h + \sin^2 2d_h),$$

$$\tilde{\gamma} = \tfrac{1}{32}(3 - \cos 4h - 2\cos^2 2h \cos 4d_h).$$

This transfer matrix possesses four nonzero eigenvalues: the eigenvalue $\lambda_0 = 1$, two degenerated eigenvalues $\lambda_{1,2} = \cos^2 2d_h \cos 2h$ [coincide with the eigenvalue λ_1 for the two-point transfer matrix, Eq. (7.18)], and the eigenvalue $\lambda_3 = \cos^2 2d_h \cos^2 2h$. Note that $\lambda_{1,2}$ are identical to the second-largest eigenvalue [Eq. (7.18)] of the transfer matrix (7.17). This implies that the decay rate of the correlations between operators with the two-point and four-point supports coincide.

VIII. CONCLUSIONS

In the current paper, we have explored two-dimensional lattice models featuring partial spatiotemporal symmetry. The study revealed that for partially dual-unitary models, non-trivial correlations exist along the light-cone edges in the space-time grid. We have expressed these correlations through

the expectation values of powers of a low-dimensional transfer matrix. On the other hand, fully dual-unitary models exhibit ultralocal correlations that completely vanish after a finite time. These findings corroborate earlier observations [10] indicating that (fully) dual-unitary models constitute a max-imally chaotic class of systems.

As an illustration, we applied these findings to the coupled quantum cat maps and the kicked Ising spin lattice. For these models we have derived an explicit formula for the spectrum of the transfer operator $\hat{T}$, enabling us to determine decay rates of correlation functions for operators with two-point and four-point supports. Remarkably, the second-largest eigenval-ues of $\hat{T}$ attain a simple structure—it is provided here by the second-largest eigenvalue of the transfer operator for the corresponding one-dimensional model, multiplied by some reducing factor [Eqs. (7.11) and (7.18)]. The absolute value of this factor depends on the coupling in nondual directions and is bounded from above by one. This demonstrates that the inclusion of an extra spatial dimension generally en-hances the decay rate of the correlation function. Note also that the transfer matrix at a certain choice of the basis vec-tors can be presented in the $L \times L$ block form (the typical structures of the four- and eight-point transfer matrices are shown in Fig. 12). In the case of the coupled cat map model, the structure of the four-point transfer matrix can be seen as a matrix of permutations, while the eight-point transfer matrix represents a hierarchy of permutations on different scales. Such hierarchy is clearly seen for the transfer ma-trices plotted for the kicked Ising spin model [Fig. 12(b)]. The eight-point transfer matrix has a block-hierarchical struc-ture, which is also known as Parisi matrix, typical for spin models.

It is worth noticing that the above results can be straightfor-wardly extended to lattice models with arbitrary dimensions $D > 2$. Assuming that the dual-unitarity holds for at least two spatial dimensions (e.g., 1, 2), we can conclude that the correlation function can take nontrivial values

$$C(\boldsymbol{r}, t) \neq 0, \quad \boldsymbol{r} = (n_1, n_2, \dots n_D) \tag{8.1}$$

if and only if the following three inequalities hold:

$$|t| \geqslant \sum_{i=1}^{D} |n_i|, \tag{8.2}$$

$$|n_1| \geqslant |t| + \sum_{i \neq 1}^{D} |n_i|, \tag{8.3}$$

$$|n_2| \geqslant |t| + \sum_{i \neq 2}^{D} |n_i|. \tag{8.4}$$

As these are satisfied only at a single point, $t = 0, \boldsymbol{r} = 0$, all correlations in this case are ultralocal, meaning they vanish identically after a finite time. If, however, the dual unitarity holds solely for a single spatial dimension, then only the first two inequalities are satisfied. In this case, the nontrivial correlations emerge along the line $|t| = |n_1|, n_i = 0, i \neq 1$. As in the two-dimensional case, $C(\boldsymbol{r}, t)$ can be expressed through a transfer operator, whose dimension is determined by the size of the local operator's support.

Finally, we note that in this article, among the calculation of the correlation function, we also established the neces-sary conditions for the quantum map duality property (the Hadamard property of the matrices $u[g]$ and $u[f]$), and we were not concerned with the clarification of the sufficient conditions for the duality. The obvious strict equivalence $f = g$ leading to the duality can be significantly relaxed: As we demonstrated in Sec. VII the duality holds for a rather wide class of functions. From our derivation we can say that the duality holds for the functions those f and g, which are in the relation $f(s, s') - g(s, s') = A(s) + B(s')$, where $A(s)$ and $B(s)$ are arbitrary real-valued functions. Nevertheless, the problem of finding a class of functions, which guarantees duality, is of interest and is the topic for future research.

APPENDIX A: QUANTUM CIRCUIT REPRESENTATION OF 2D DUAL-UNITARY COUPLED MAPS

In this Appendix, we show that a dual-unitary kicked quan-tum map on 2D lattice can be represented as a 2D quantum circuit with a ternary unitary gate operator $\mathcal{U}^{\text{gate}} \in \text{End}(\mathcal{H}^{\otimes 4})$.

Assuming that the lattice has even dimensions M, N, we split the interaction part of the evolution (4.6) into two terms, $U_I = U_I^e U_I^o$,

$$\langle \boldsymbol{s} | U_I^e | \boldsymbol{s}' \rangle \equiv \delta(\boldsymbol{s}, \boldsymbol{s}') \prod_{n=1}^{N/2} \prod_{m=1}^{M/2} [e^{\mathrm{i} f_v(s_{2n,2m}; s_{2n+1,2m}) + \mathrm{i} f_h(s_{2n,2m}; s_{2n,2m+1})}], \tag{A1}$$

$$\langle \boldsymbol{s} | U_I^o | \boldsymbol{s}' \rangle \equiv \delta(\boldsymbol{s}, \boldsymbol{s}') \prod_{n=1}^{N/2} \prod_{m=1}^{M/2}$$
$$\times [e^{\mathrm{i} f_v(s_{2n-1,2m-1}; s_{2n,2m-1}) + \mathrm{i} f_h(s_{2n-1,2m-1}; s_{2n-1,2m})}], \tag{A2}$$

where the sum runs over even and odd lattice sites, respec-tively. The even powers of the Floquet operator (3.2) can be written in the form

$$U^{2t} = (U_K U_I)^{2t} = U_I^{e\dagger} \left[U_I^e U_K U_I^e U_I^o U_K U_I^o \right]^t U_I^e, \tag{A3}$$

where we split the interaction part of the evolution into the odd and even parts of the lattice. The two parts of the evolution are given by

$$U_e = U_I^e U_K U_I^e = \bigotimes_{(i,j) \in \{1,\dots,N/2\}} \mathcal{U}_{(2i,2j)}^{\text{gate}}, \tag{A4}$$

$$U_o = U_I^o U_K U_I^o = \bigotimes_{(i,j) \in \{1,\dots,N/2\}} \mathcal{U}_{(2i+1,2j+1)}^{\text{gate}}, \tag{A5}$$

where $\mathcal{U}_{(m,n)}^{\text{gate}}$ is the ternary unitary operator $\mathcal{U}^{\text{gate}}$ acting on the site (m, n) of the lattice, see Fig. 13(a). Explicitly it is given
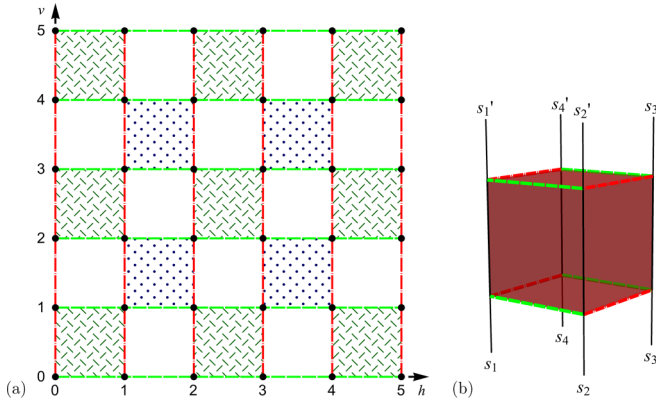
FIG. 13. (a) Two-dimensional lattice of interacting particles. The green-dashed lines correspond to the interactions defined by the function f_h, and the red dot-dashed lines to the function f_v. The squares marked by different shadowing correspond to even U_e and odd parts U_o of the evolution, see Eqs. (A4) and (A5). (b) Schematics of the ternary unitary operator $\mathcal{U}^{\text{gate}}$, which includes among the particle-particle interactions (green and red dashed edges of the cube) also one time-step propagation (the vertical edges), see Eqs. (A6) and (A7).

by $L^4 \times L^4$ matrix with the entries

$$\langle s_1 s_2 s_3 s_4 | \mathcal{U}^{\text{gate}} | s_4' s_3' s_2' s_1' \rangle = \frac{1}{L^2} e^{i\mathcal{F}(s,s')}, \quad \text{(A6)}$$

$$\begin{aligned}
\mathcal{F} &= f_v(s_1, s_2) + f_v(s_3, s_4) + f_h(s_2, s_3) + f_h(s_4, s_1) \\
&\quad + f_v(s_1', s_2') + f_v(s_3', s_4') + f_h(s_2', s_3') + f_h(s_4', s_1') \\
&\quad + g(s_1, s_1') + g(s_2, s_2') + g(s_3, s_3') + g(s_4, s_4'), \quad \text{(A7)}
\end{aligned}$$

corresponding to 12 edges of the cube, see Fig. 13(b).

Due to the forms of the operators U_e, U_o, the equation (A3) effectively represents the time-evolution as a 2D quantum circuit with a ternary unitary gate operator, akin to the approach in the work [41]. Importantly, the unitary gate (A7) allows for spreading onto the neighboring sites only. Indeed, it is straightforward to see that for a local operator a_j localized on the site $j \in \{1, 2, 3, 4\}$ we have

$$\mathcal{U}^{\text{gate}}[a_j \otimes I \otimes I \otimes I](\mathcal{U}^{\text{gate}})^\dagger = A \otimes I, \quad \text{(A8)}$$

where A is localized on the sites j, $(j \pm 1)\bmod 4$ and the last unite operator I on the site $(j + 2)\bmod 4$, respectively. This accounts for the ultralocal correlations in our model, distinguishing it from the one featuring a generic ternary unitary gate as described in [41].

APPENDIX B: THE SPIN STRUCTURES OBTAINED BY APPLICATION OF THE CONTRACTION RULES

Multiple applications of the contraction rules formulated in Sec. III to the original spin structure in the case of the two-dimensional partially dual map (the horizontal direction is dual to the time direction) and for $T \gg M, N$ generates a number of nontrivial structures. In the generic case of the eight-point correlation function, there are three (up to the mirror transformation $n \to N - n$) nontrivial final structures (Fig. 14) taking place at $v = T, T + 1, T + 2$ [see Eq. (4.7)]. Further analysis shows that only the case $v = T + 1$ corresponds to the nontrivial correlation function. Moreover, the structure similar to the one shown in Fig. 14(b) reduces to those in Fig. 8(b). These conclusions follow from the explicit summation of the correlated spins (red balls) in the vicinity of the boundaries (green balls).

On the upper boundary of the structure shown in Fig. 14(a), the summation over the correlated spins $s_{N,1,0}$, $s_{N,2,0}$, $s_{3,1,0}$, $s_{3,2,0}$ has to be done according to the following scheme (only the spins with $m = 1$ are shown)

$$
\begin{array}{ccccccc}
t = 0 & s_{N,1,0} \xrightarrow{f_v} & \langle \bar{s}_{1,1,0} | \, \mathbf{q}_1 \, | \underline{s}_{1,1,0} \rangle & \xrightarrow{f_v} & \langle \bar{s}_{2,1,0} | \, \mathbf{q}_2 \, | \underline{s}_{2,1,0} \rangle & \xrightarrow{f_v} & s_{3,1,0} \\
& & \Big\uparrow g & & \Big\uparrow g & & \\
t = 1 & & s_{1,1,1} \xrightarrow{\quad f_v \quad} & (\bar{s}_{2,1,1}, \underline{s}_{2,1,1}) & \xrightarrow{\quad f_v \quad} & \cdots &
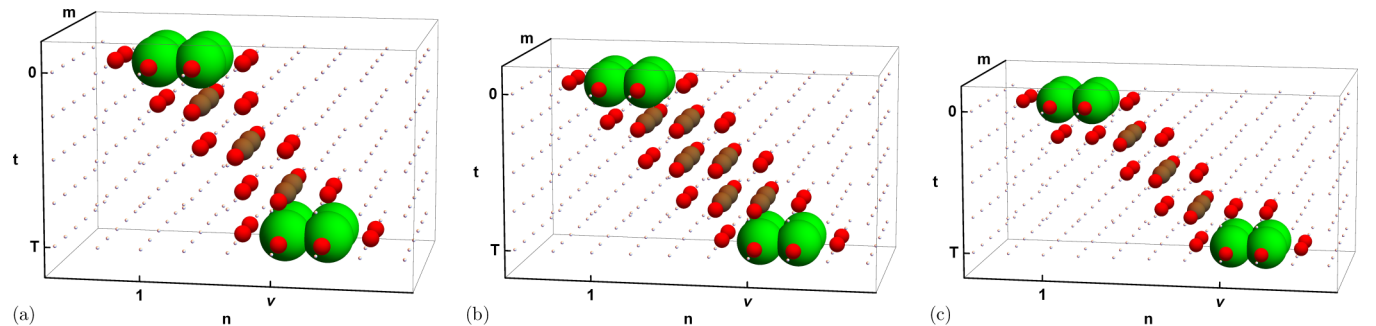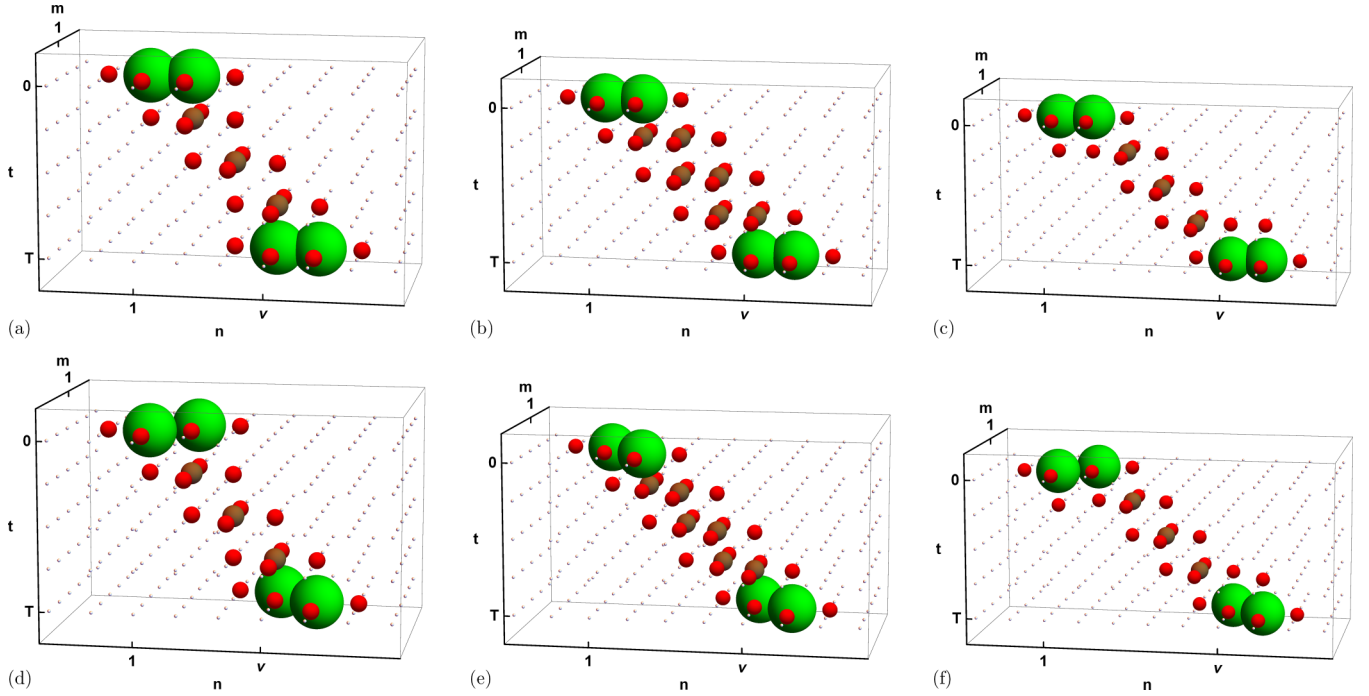\end{array} \quad \text{(B1)}
$$

FIG. 14. The spin structures generated after the application of the contraction rules in the temporal and the horizontal directions at $T = 4$ ($M, N \gg T$) and (a) $v = 4$, (b) $v = 5$, (c) $v = 6$.

FIG. 15. The spin structures generated after the application of the contraction rules in the temporal and the horizontal directions at $T = 4$ ($M, N \gg T$) when only four from eight operators q_ℓ are different from $\mathbb{1}$. The mutual positions of the operators q_ℓ are different at each plot and [(a),(d)] $\nu = 4$, [(b),(e)] $\nu = 5$, [(c),(f)] $\nu = 6$.

The arrows on this scheme show the order of indexes in the corresponding functions (f_ν of g), from left to right. The horizontal interactions are not shown, while the presence of the horizontal interactions after summation results in the correlation of the spins $\bar{s}_{1,1,0}$ and $\underline{s}_{1,1,0}$. Thus, on the next turn, summation over the spin $s_{1,1,1}$ leads to the correlation of $\bar{s}_{2,1,1}$ and $\underline{s}_{2,1,1}$, which cuts the spin bridge and the correlation function becomes trivial (the same arguing works for the spins with $m = 2$).

The spin structure in Fig. 14(c) has to be analysed starting from the bottom. To formulate the contraction rules in a symmetric manner we have introduced the additional matrices U_I into $\Phi(\bar{s}_T, \underline{s}_T)$, so that the product $\Phi(\bar{s}_T, \underline{s}_T)\bar{I}_I(\bar{s}_T, \underline{s}_T)$ reduces to the scalar product $\langle \bar{s}_T | \underline{\Sigma} | \underline{s}_T \rangle$, where all spins on the level $t = T$ are correlated and does not interact horizontally. Therefore summation over the spins $s_{T+1,1,T}$ and $s_{T+1,2,T}$ results in the correlation of the spin pairs $\bar{s}_{T+1,1,T-1}$, $\underline{s}_{T+1,1,T-1}$ and $\bar{s}_{T+1,2,T-1}$, $\underline{s}_{T+1,2,T-1}$, which again breaks the spin bridge. The very same arguments allow us to reduce the spin structure in Fig. 14(b) to obtain the one in Fig. 8(b).

For completeness, we also plotted the structures obtained after the application of the contraction rules for the case corresponding to the four-point correlation function with various mutual positions of the operators $\mathbf{q}_\ell$, see Fig. 15. Additional analysis shows that only one of them shown in Fig. 15(b)

generates a nontrivial correlation function. It can be reduced to the structure in Fig. 7(b).

APPENDIX C: EXPLICIT EXPRESSIONS FOR THE CORRELATION FUNCTION IN THE SPIN-CHAIN MODEL (SEC. VII B)

The correlation function calculated in Eq. (7.19) take nonzero values for particular choices of the operators $\mathbf{q}_i$: $\mathbf{q}_1 = \hat{\sigma}^z$, $\mathbf{q}_6 = \hat{\sigma}^y$, $\mathbf{q}_2 = \hat{\sigma}^x$, $\hat{\sigma}^y$, $\mathbf{q}_5 = \hat{\sigma}^x$, $\hat{\sigma}^z$, totally four combinations. We use the standard definition of the Pauli matrices,

$$\hat{\sigma}^z = \begin{pmatrix} 1 & 0 \\ 0 & -1 \end{pmatrix}, \quad \hat{\sigma}^x = \begin{pmatrix} 0 & 1 \\ 1 & 0 \end{pmatrix}, \quad \hat{\sigma}^y = \begin{pmatrix} 0 & -i \\ i & 0 \end{pmatrix}. \tag{C1}$$

The correlation function is

$$C(T) = -2\lambda_1^{T-2} \cos^4 2d_h \times (\mathrm{I}) \times (\mathrm{II}), \tag{C2}$$

where the factors (I), (II) take the following values:

$$(\mathrm{I}) = \begin{cases} \sin 2h & \mathbf{q}_2 = \hat{\sigma}^x, \\ -\cos 2h & \mathbf{q}_2 = \hat{\sigma}^y, \end{cases} \tag{C3}$$

$$(\mathrm{II}) = \begin{cases} \sin 2h & \mathbf{q}_5 = \hat{\sigma}^x, \\ -\cos 2h & \mathbf{q}_5 = \hat{\sigma}^z. \end{cases} \tag{C4}$$

[1] F. Haake, *Quantum Signatures of Chaos*, Springer Series in Synergetics, 3rd ed. (Springer, New York, 2010).

[2] T. Guhr, A. Müller-Groeling, and H. A. Weidenmüller, Random-matrix theories in quantum physics: Common concepts, Phys. Rep. **299**, 189 (1998).

[3] M. P. Fisher, V. Khemani, A. Nahum, and S. Vijay, Random quantum circuits, Annu. Rev. Condens. Matter Phys. **14**, 335 (2023).

[4] B. Gutkin and V. Osipov, Classical foundations of many-particle quantum chaos, Nonlinearity **29**, 325 (2016).

[5] B. Gutkin, P. Cvitanović, R. Jafari, A. K. Saremi, and L. Han, Linear encoding of the spatiotemporal cat, Nonlinearity **34**, 2800 (2021).

[6] H. Liang and P. Cvitanović, A chaotic lattice field theory in one dimension, J. Phys. A: Math. Theor. **55**, 304002 (2022).

[7] I. Fouxon and B. Gutkin, Local correlations in coupled cat maps with space-time duality, J. Phys. A: Math. Theor. **55**, 504004 (2022).

[8] M. Akila, D. Waltner, B. Gutkin, and T. Guhr, Particle-time duality in the kicked Ising spin chain, J. Phys. A **49**, 375101 (2016).

[9] B. Bertini, P. Kos, and T. Prosen, Exact spectral form factor in a minimal model of many-body quantum chaos, Phys. Rev. Lett. **121**, 264101 (2018).

[10] B. Bertini, P. Kos, and T. Prosen, Entanglement spreading in a minimal model of maximal many-body quantum chaos, Phys. Rev. X **9**, 021033 (2019).

[11] B. Gutkin, P. Braun, M. Akila, D. Waltner, and T. Guhr, Exact local correlations in kicked chains, Phys. Rev. B **102**, 174307 (2020).

[12] B. Bertini, P. Kos, and T. Prosen, Exact correlation functions for dual-unitary lattice models in $1 + 1$ dimensions, Phys. Rev. Lett. **123**, 210601 (2019).

[13] R. M. Milbradt, L. Scheller, C. Aßmus, and C. B. Mendl, Ternary unitary quantum lattice models and circuits in $2 + 1$ dimensions, Phys. Rev. Lett. **130**, 090601 (2023).

[14] M. Mestyán, B. Pozsgay, and I. M. Wanless, Multi-directional unitarity and maximal entanglement in spatially symmetric quantum states, SciPost Phys. **16**, 010 (2024).

[15] G. M. Sommers, S. Gopalakrishnan, M. Gullans, and D. A. Huse, Zero-temperature entanglement membranes in quantum circuits, arXiv:2404.02975.

[16] S. A. Rather, S. Aravinda, and A. Lakshminarayan, Creating ensembles of dual unitary and maximally entangling quantum evolutions, Phys. Rev. Lett. **125**, 070501 (2020).

[17] S. Gopalakrishnan and A. Lamacraft, Unitary circuits of finite depth and infinite width from quantum channels, Phys. Rev. B **100**, 064309 (2019).

[18] R. Pal and A. Lakshminarayan, Entangling power of time-evolution operators in integrable and nonintegrable many-body systems, Phys. Rev. B **98**, 174304 (2018).

[19] P. Braun, D. Waltner, M. Akila, B. Gutkin, and T. Guhr, Transition from quantum chaos to localization in spin chains, Phys. Rev. E **101**, 052201 (2020).

[20] L. Piroli, B. Bertini, J. I. Cirac, and T. C. V. Prosen, Exact dynamics in dual-unitary quantum circuits, Phys. Rev. B **101**, 094304 (2020).

[21] B. Bertini, P. Kos, and T. Prosen, Operator entanglement in local quantum circuits I: Chaotic dual-unitary circuits, SciPost Phys. **8**, 067 (2020).

[22] P. Kos, B. Bertini, and T. C. V. Prosen, Correlations in perturbed dual-unitary circuits: Efficient path-integral formula, Phys. Rev. X **11**, 011022 (2021).

[23] T. Zhou and A. Nahum, Entanglement membrane in chaotic many-body systems, Phys. Rev. X **10**, 031066 (2020).

[24] J. Avan, V. Caudrelier, A. Doikou, and A. Kundu, Lagrangian and hamiltonian structures in an integrable hierarchy and space-time duality, Nucl. Phys. B **902**, 415 (2016).

[25] D. Goyeneche, D. Alsina, J. I. Latorre, A. Riera, and K. Życzkowski, Absolutely maximally entangled states, combinatorial designs, and multiunitary matrices, Phys. Rev. A **92**, 032316 (2015).

[26] S. Aravinda, S. A. Rather, and A. Lakshminarayan, From dual-unitary to quantum bernoulli circuits: Role of the entangling power in constructing a quantum ergodic hierarchy, Phys. Rev. Res. **3**, 043034 (2021).

[27] A. Chan, A. De Luca, and J. T. Chalker, Spectral lyapunov exponents in chaotic and localized many-body quantum systems, Phys. Rev. Res. **3**, 023118 (2021).

[28] P. W. Claeys and A. Lamacraft, Maximum velocity quantum circuits, Phys. Rev. Res. **2**, 033032 (2020).

[29] M. Borsi and B. Pozsgay, Construction and the ergodicity properties of dual unitary quantum circuits, Phys. Rev. B **106**, 014302 (2022).

[30] M. Ippoliti and V. Khemani, Postselection-free entanglement dynamics via spacetime duality, Phys. Rev. Lett. **126**, 060501 (2021).

[31] P. W. Claeys, M. Henry, J. Vicary, and A. Lamacraft, Exact dynamics in dual-unitary quantum circuits with projective measurements, Phys. Rev. Res. **4**, 043212 (2022).

[32] Ž. Krajnik and T. Prosen, Kardar–Parisi–Zhang physics in integrable rotationally symmetric dynamics on discrete space–time lattice, J. Stat. Phys. **179**, 110 (2020).

[33] T.-C. Lu and T. Grover, Spacetime duality between localization transitions and measurement-induced transitions, PRX Quantum **2**, 040319 (2021).

[34] T. Prosen, Many-body quantum chaos and dual-unitarity round-a-face, Chaos **31**, 093101 (2021).

[35] A. Lerose, M. Sonner, and D. A. Abanin, Influence matrix approach to many-body Floquet dynamics, Phys. Rev. X **11**, 021040 (2021).

[36] M. Ippoliti, T. Rakovszky, and V. Khemani, Fractal, logarithmic, and volume-law entangled nonthermal steady states via spacetime duality, Phys. Rev. X **12**, 011045 (2022).

[37] F. Fritzsch and T. Prosen, Eigenstate thermalization in dual-unitary quantum circuits: Asymptotics of spectral functions, Phys. Rev. E **103**, 062133 (2021).

[38] R. Suzuki, K. Mitarai, and K. Fujii, Computational power of one-and two-dimensional dual-unitary quantum circuits, Quantum **6**, 631 (2022).

[39] A. Flack, B. Bertini, and T. Prosen, Statistics of the spectral form factor in the self-dual kicked Ising model, Phys. Rev. Res. **2**, 043403 (2020).

[40] B. Bertini, P. Kos, and T. Prosen, Random matrix spectral form factor of dual-unitary quantum circuits, Commun. Math. Phys. **387**, 597 (2021).

[41] C. Jonay, V. Khemani, and M. Ippoliti, Triunitary quantum circuits, Phys. Rev. Res. **3**, 043046 (2021).

[42] M. Akila, D. Waltner, B. Gutkin, P. Braun, and T. Guhr, Semiclassical identification of periodic orbits in a quantum many-body system, Phys. Rev. Lett. **118**, 164101 (2017).

[43] M. Akila, B. Gutkin, P. Braun, D. Waltner, and T. Guhr, Semiclassical prediction of large spectral fluctuations in interacting kicked spin chains, Ann. Phys. **389**, 250 (2018).

[44] V. Arnold and A. Avez, *Ergodic Problems of Classical Mechanics* (Addison-Wesley, Redwood City, CA, 1989).

[45] J. Hannay and M. Berry, Quantization of linear maps on a torus-fresnel diffraction by a periodic grating, Physica D **1**, 267 (1980).

[46] A. M. F. Rivas, M. Saraceno, and A. M. O. de Almeida, Quantization of multidimensional cat maps, Nonlinearity **13**, 341 (2000).

[47] T. Prosen, Exact Time-correlation functions of quantum Ising chain in a kicking transversal magnetic field: Spectral analysis of the adjoint propagator in Heisenberg picture, Prog. Theor. Phys. Suppl. **139**, 191 (2000).

[48] C. Pineda, T. Prosen, and E. Villaseñor, Two dimensional kicked quantum Ising model: Dynamical phase transitions, New J. Phys. **16**, 123044 (2014).